Tau reduction prevents Aβ-induced axonal transport deficits by blocking activation of GSK3β

Keith A. Vossel,[1,2] Jordan C. Xu,[1] Vira Fomenko,[1] Takashi Miyamoto,[1,2] Elsa Suberbielle,[1,2] Joseph A. Knox,[1] Kaitlyn Ho,[1] Daniel H. Kim,[1] Gui-Qiu Yu,[1] and Lennart Mucke[1,2]

[1]Gladstone Institute of Neurological Disease, San Francisco, CA 94158
[2]Department of Neurology, University of California, San Francisco, San Francisco, CA 94158

Axonal transport deficits in Alzheimer's disease (AD) are attributed to amyloid β (Aβ) peptides and pathological forms of the microtubule-associated protein tau. Genetic ablation of tau prevents neuronal overexcitation and axonal transport deficits caused by recombinant Aβ oligomers. Relevance of these findings to naturally secreted Aβ and mechanisms underlying tau's enabling effect are unknown. Here we demonstrate deficits in anterograde axonal transport of mitochondria in primary neurons from transgenic mice expressing familial AD-linked forms of human amyloid precursor protein. We show that these deficits depend on $A\beta_{1-42}$ production and are prevented by tau reduction. The copathogenic effect of tau did not depend on its microtubule binding, interactions with Fyn, or potential role in neuronal development. Inhibition of neuronal activity, *N*-methyl-D-aspartate receptor function, or glycogen synthase kinase 3β (GSK3β) activity or expression also abolished Aβ-induced transport deficits. Tau ablation prevented Aβ-induced GSK3β activation. Thus, tau allows Aβ oligomers to inhibit axonal transport through activation of GSK3β, possibly by facilitating aberrant neuronal activity.

Introduction

Alzheimer's disease (AD) is the most common neurodegenerative disease of aging and currently has no cure. Two key factors in AD pathogenesis are amyloid β (Aβ) peptides, derived from the human amyloid precursor protein (hAPP), and the microtubule-associated protein tau. Despite intense investigation, the precise mechanisms by which these factors impair neuronal functions remain uncertain.

Axonal transport is critical for neuronal function and survival and is impaired by Aβ (Hiruma et al., 2003; Rui et al., 2006; Decker et al., 2010; Wang et al., 2010; Calkins and Reddy, 2011; Tang et al., 2012). Pathogenic forms of tau can also inhibit axonal transport (Zhang et al., 2004; Ittner et al., 2008; LaPointe et al., 2009; Kanaan et al., 2011), and pathologically modified tau species that inhibit axonal transport in cell cultures are found in AD brains (Kanaan et al., 2011; Shahpasand et al., 2012). We previously showed that Aβ requires endogenous tau to inhibit the axonal transport of mitochondria and TrkA receptors, establishing a direct link between Aβ and tau in the impairment of axonal transport (Vossel et al., 2010). This finding added to growing evidence that tau enables Aβ-induced neuronal dysfunction at multiple levels of complexity, including DNA double-strand breaks (Suberbielle et al., 2013), cell-cycle reentry (Seward et al., 2013), cytoskeletal disruption (King et al., 2006; Jin et al., 2011; Zempel et al., 2013), cell death (Rapoport et al., 2002; Leroy et al., 2012; Nussbaum et al., 2012), synaptic dysfunction (Roberson et al., 2011; Shipton et al., 2011), aberrant network excitability (Roberson et al., 2007, 2011; Ittner et al., 2010), mortality (Roberson et al., 2007, 2011; Ittner et al., 2010; Leroy et al., 2012), and cognitive and behavioral alterations (Roberson et al., 2007, 2011; Ittner et al., 2010; Leroy et al., 2012).

Although overall tau reduction is an attractive therapeutic approach for AD and epilepsy (Morris et al., 2011; DeVos et al., 2013; Holth et al., 2013; Gheyara et al., 2014), a more detailed understanding of how tau enables Aβ-induced neuronal dysfunction will be critical for the development of more specific

Correspondence to Keith A. Vossel: kvossel@gladstone.ucsf.edu; or Lennart Mucke: lmucke@gladstone.ucsf.edu

Abbreviations used in this paper: Aβ, amyloid β; AD, Alzheimer's disease; ANOVA, analysis of variance; $[Ca^{2+}]_i$, intracellular calcium; D-AP5, D-(−)-2-amino-5-phosphonopentanoic acid; DIV, day in vitro; DPBS, Dulbecco's phosphate-buffered saline; GSK3β, glycogen synthase kinase 3β; GSM, γ-secretase modulator; hAPP, human amyloid precursor protein; NMDAR, *N*-methyl-D-aspartate receptor; PS1, presenilin 1; TTX, tetrodotoxin.

The Rockefeller University Press $30.00
J. Cell Biol. Vol. 209 No. 3 419–433
www.jcb.org/cgi/doi/10.1083/jcb.201407065

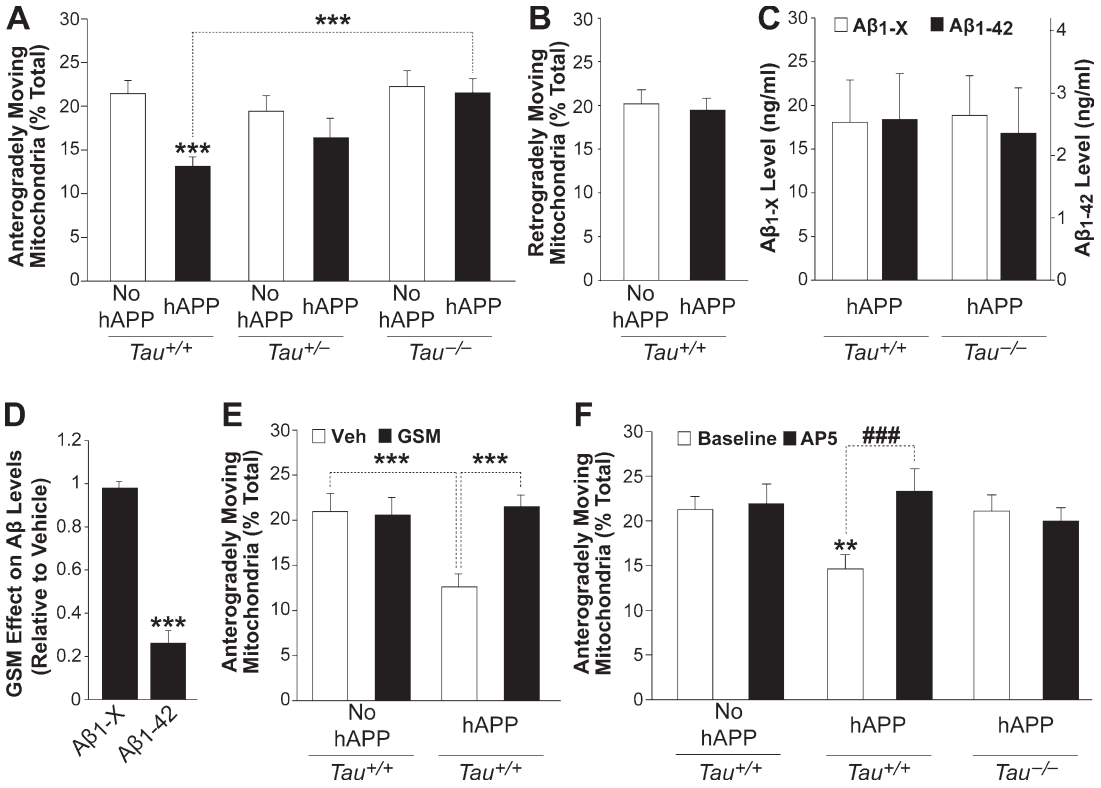

Figure 1. **Tau ablation, γ-secretase modulation, and NMDAR blockade each ameliorates deficits in anterograde axonal transport of mitochondria in Aβ-producing primary hippocampal neurons from hAPP-J20 mice.** (A and B) Anterograde (A) and retrograde (B) axonal transport in neurons from mice of the indicated genotypes. *n* = 25–51 axons from three to five mice and three to six independent sessions for each genotype at DIV 10–14. ***, P < 0.001 versus *Tau*$^{+/+}$ or as indicated by bracket (Dunnett's test). (C) Levels of $A\beta_{1\text{-}x}$ and $A\beta_{1\text{–}42}$ in the medium, measured by ELISA, were roughly equivalent to 4 and 0.55 nM of Aβ monomer, respectively. *n* = 4–9 wells from three to five mice per genotype at DIV 14. (D) Aβ levels in DIV 14 medium from hAPP/*Tau*$^{+/+}$ neurons treated with a GSM (BMS-893204; 100 nM final concentration) from DIV 1–14, relative to Aβ levels in replicate cultures treated with vehicle (DMSO; 0.001% final concentration). *n* = 5–6 wells from four mice per treatment. ***, P < 0.001 versus vehicle (arbitrarily defined as 1.0) by one-sample *t* test. (E) Axonal transport in neurons of the indicated genotypes treated with GSM (100 nM) or vehicle (Veh; DMSO) over 12–14 d. *n* = 23–29 axons from three mice per genotype and treatment from three independent sessions at DIV 12–14. ***, P < 0.001 (Dunnett's test). (F) Axonal transport in neurons of the indicated genotypes before (baseline) and after treatment with the selective NMDAR antagonist D-AP5 (100 µM final concentration; for 1 h) at DIV 12–14. *n* = 22–24 axons from three mice for each genotype at DIV 12–14. **, P < 0.01 versus *Tau*$^{+/+}$ baseline (Dunnett's test); ###, P < 0.001 (paired *t* test, Bonferroni). Data are means ± SEM.

tau-targeted therapies. Reducing or ablating tau is well tolerated in mice (Roberson et al., 2007; Yuan et al., 2008; Morris et al., 2011, 2013; DeVos et al., 2013), but, in culture, tau-deficient neurons display delayed maturation of axons (Dawson et al., 2001), and tau knockdown during prenatal stages inhibits neuronal migration (Sapir et al., 2012). Whether tau's enabling role in Aβ-induced axonal transport deficits requires its microtubule-binding capacity, its function during neural development, or other activities is unknown.

In this study, we used tau ablation, knockdown, and reconstitution to investigate mechanisms by which tau enables Aβ-induced deficits of mitochondrial axonal transport. We found that mutant tau with markedly reduced microtubule-binding capacity still enabled Aβ-induced axonal transport deficits. Tau ablation prevented Aβ-induced activation of glycogen synthase kinase 3β (GSK3β), a kinase that is essential for Aβ-induced axonal transport deficits (Rui et al., 2006; Decker et al., 2010; Tang et al., 2012). These observations suggest a role for tau in Aβ-induced neuronal dysfunction that is independent of microtubule binding and upstream of GSK3β activation.

Results

Axonal transport deficits in neurons from hAPP mice depend on $A\beta_{1\text{-}42}$, tau, and *N*-methyl-D-aspartate receptor (NMDAR) function

We previously compared acute effects of exogenously applied recombinant Aβ oligomers on axonal transport in wild-type and tau-deficient mouse hippocampal neurons (Vossel et al., 2010). To investigate the effects of naturally secreted Aβ on axonal transport, we measured axonal transport of mitochondria in hippocampal neurons from mice of six different genotypes (*Tau*$^{+/+}$, *Tau*$^{+/–}$, *Tau*$^{–/–}$, hAPP/*Tau*$^{+/+}$, hAPP/*Tau*$^{+/–}$, and hAPP/*Tau*$^{–/–}$). hAPP/Aβ expression impaired anterograde axonal transport in *Tau*$^{+/+}$ neurons, but not in *Tau*$^{+/–}$ or *Tau*$^{–/–}$ neurons (Fig. 1 A). Retrograde mitochondrial motility was not affected by neuronal expression of hAPP/Aβ (Fig. 1 B). The velocity of moving mitochondria was also unaffected by hAPP/Aβ expression and tau reduction (Fig. S1, A and B), consistent with findings obtained in neuronal cultures exposed to recombinant Aβ oligomers

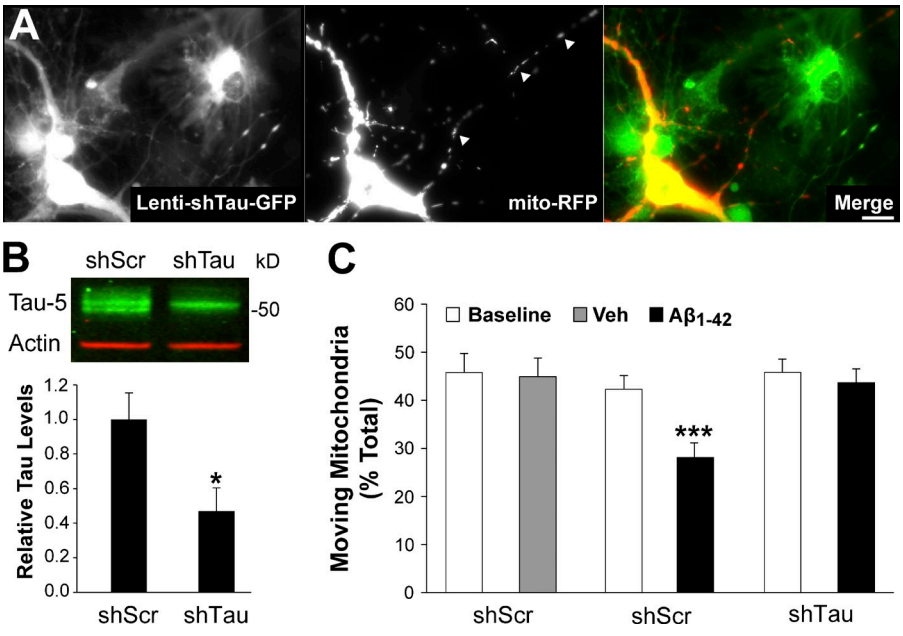

Figure 2. **Knocking down tau with lentivirus-shRNA prevents deficits in axonal transport of mitochondria in wild-type (*Tau*$^{+/+}$) primary hippocampal neurons caused by exposure to Aβ oligomers.** (A) Neurons were transduced with lentivirus expressing anti-tau shRNA and EGFP (Lenti-shTau-GFP; left, monochrome; right, green) on DIV 0 and transfected with a mitochondrial marker (mito-RFP; middle, monochrome; right, red) at DIV 6. Arrowheads indicate mitochondria in axon. Bar, 20 µm. (B) Total tau levels in neurons transduced with Lenti-shTau-GFP (shTau) or a similar construct expressing a scrambled shRNA (shScr) were determined by Western blot analysis with the Tau-5 antibody. Top, representative blot; bottom, quantitation of blot signals. Mean Tau/actin ratios in scrambled shRNA–expressing neurons were arbitrarily defined as 1.0. n = 6–7 wells from four to five experiments per condition at DIV 14. *, $P < 0.05$ (unpaired t test). (C) The percentage of mitochondria moving anterogradely or retrogradely relative to all mitochondria in the axons of neurons transduced as in A and B before (baseline) and 10–60 min after adding vehicle (Veh) or $A\beta_{1–42}$ oligomers (final concentration equivalent to 2-µM monomer) to the medium. n = 25–40 axons recorded during three to four independent sessions at 12–14 DIV. ***, $P < 0.001$ (paired t test, Bonferroni). Data are means ± SEM.

(Vossel et al., 2010). $A\beta_{1-x}$ and $A\beta_{1–42}$ levels in the growth medium of neurons from hAPP transgenic mice were in the low nanomolar range (monomeric equivalent) and were not altered by ablating tau (Fig. 1 C). Thus, low concentrations of naturally secreted Aβ recapitulate the tau-dependent effects of recombinant Aβ peptides on anterograde axonal transport.

Mitochondrial fission and fusion are critical for proper transport and distribution of mitochondria along the axon, and both tau and Aβ have been implicated in fission–fusion imbalance (Wang et al., 2008, 2009; Cho et al., 2009; DuBoff et al., 2012). However, neither hAPP/Aβ expression nor tau reduction altered the length of axonal mitochondria (Fig. S1 C), suggesting that mitochondrial transport deficits in axons of hAPP transgenic neurons are not caused by alterations in mitochondrial fission or fusion.

We next used a γ-secretase modulator (GSM; BMS-893204) to test whether the observed axonal transport deficits in hAPP transgenic neurons depend specifically on $A\beta_{1–42}$ production. BMS-893204 selectively reduces the production of $A\beta_{1–42}$ by directing γ-secretase to cleave APP at sites that produce shorter forms of Aβ (Boy et al., 2013). GSM treatment reduced $A\beta_{1–42}$ levels in the medium by 75% without affecting $A\beta_{1-x}$ (Fig. 1 D) or hAPP levels (Fig. S2, A and B). The GSM did not increase the production of hAPP C-terminal fragments, confirming that it did not act like a γ-secretase inhibitor (Fig. S2 A). GSM treatment also prevented deficits in anterograde axonal transport in hAPP/*Tau*$^{+/+}$ neurons without affecting axonal transport in *Tau*$^{+/+}$ neurons (Fig. 1 E). Thus, axonal transport deficits in hAPP/*Tau*$^{+/+}$ neurons depend on $A\beta_{1–42}$ production and are not likely caused by other hAPP metabolites.

Previous studies showed that NMDARs have a critical role in Aβ-induced axonal transport deficits (Decker et al., 2010; Tang et al., 2012). Consistent with these findings, treatment of cultures with the selective NMDAR antagonist D-(−)-2-amino-5-phosphonopentanoic acid (D-AP5) normalized anterograde axonal transport in hAPP/*Tau*$^{+/+}$ neurons (Fig. 1 F). However, D-AP5 treatment did not further improve axonal transport in *Tau*$^{+/+}$ or hAPP/*Tau*$^{-/-}$ neurons (Fig. 1 F). Thus, tau reduction and NMDAR blockade can each prevent Aβ from impairing axonal transport; however, they do not show additive or synergistic effects and do not appear to directly affect axonal transport in the absence of elevated Aβ levels.

Knocking down tau prevents Aβ-induced deficits in axonal transport

To assess whether the protective effects of tau reduction in our model depend on compensatory changes that could result from the genetic modification during embryonic development, we studied the effects of knocking down tau in postnatal neurons from wild-type mice. We transduced primary cultures of *Tau*$^{+/+}$ neurons with lentiviral vectors expressing either scrambled shRNA or anti-Tau shRNA. Each lentiviral vector coexpressed EGFP to indicate transduced neurons (Fig. 2 A). 14 d after infection, tau expression was roughly 50% lower in anti-Tau shRNA–expressing neurons than in scrambled shRNA–expressing neurons (Fig. 2 B). We measured axonal mitochondrial motility under baseline conditions and after adding $A\beta_{1–42}$ oligomers (characterized in Fig. S2, C and D). Consistent with observations in neurons with genetically ablated tau, knocking down tau postnatally prevented Aβ-induced defects in mitochondrial axonal transport without affecting transport at baseline (Fig. 2 C and Videos 1 and 2). Therefore, the protective effects of tau reduction are independent of developmental changes during embryonic development.

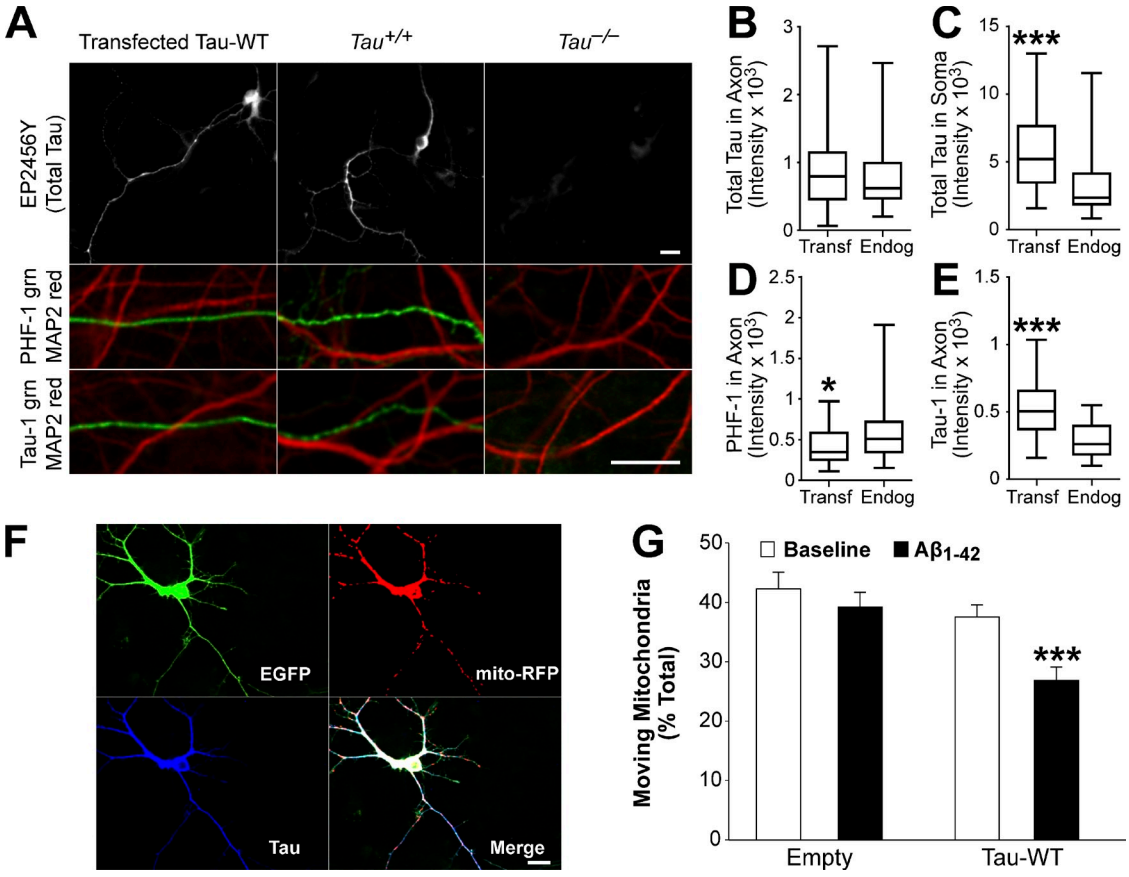

Figure 3. **Transfection with wild-type mouse tau makes primary hippocampal neurons from *Tau*$^{-/-}$ mice susceptible to Aβ-induced deficits in axonal transport.** (A) Neuronal cultures from *Tau*$^{-/-}$ mice were transfected with a cDNA encoding Tau-WT at DIV 6, fixed the next day, and immunostained for total tau (EP2456Y, white) or colabeled for the dendritic marker MAP2 (red) and for phosphorylated (PHF-1) or dephosphorylated (Tau-1) tau (green [grn]) in axons (left). To compare tau expression in transfected *Tau*$^{-/-}$ neurons with the expression of endogenous tau in *Tau*$^{+/+}$ neurons, a small number of *Tau*$^{+/+}$ neurons was co-cultured with untransfected *Tau*$^{-/-}$ neurons, followed by fixation on DIV 14 and immunostaining as in the left panels (middle). Cultures of untransfected *Tau*$^{-/-}$ neurons served as a negative control (right). (B–E) The intensity of immunostaining for total tau in the axon (B), total tau in the soma (C), and phosphorylated (D) and dephosphorylated (E) tau in the axon was compared by fluorescence microscopy in *Tau*$^{+/+}$ neurons co-cultured with *Tau*$^{-/-}$ neurons (endogenous [Endog] tau) and in *Tau*$^{-/-}$ neurons transfected (Transf) with mouse tau. n = 109–144 (B and C) and n = 36–71 (D and E) neurons per group. *, $P < 0.05$; ***, $P < 0.001$ (Mann-Whitney rank-sum test). (F) To measure axonal transport in live cells, *Tau*$^{-/-}$ neurons were transfected with EGFP (green), a mitochondrial marker (mito-RFP; red), and mouse tau. Tau was detected by immunostaining with the EP2456Y antibody (blue) after fixation. All images in F were taken after fixation. (G) The percentage of moving mitochondria in the axons of *Tau*$^{-/-}$ neurons transfected with empty plasmid or a plasmid encoding Tau-WT was measured before (baseline) and 10–60 min after adding $A\beta_{1-42}$ oligomers to the medium. n = 37 axons per group recorded during three to five independent sessions at DIV 7–8. ***, $P < 0.001$ versus corresponding baseline (paired t test, Bonferroni). Bars, 20 µm. Plots in B–E show medians, quartiles, and ranges. Data in G are means ± SEM.

Reconstituting tau expression in *Tau*$^{-/-}$ neurons restores Aβ-induced deficits in axonal transport

Next, we prepared primary neuronal cultures from *Tau*$^{-/-}$ mice and transfected them with an empty plasmid or a plasmid encoding wild-type 0N4R mouse tau (Tau-WT) on day in vitro (DIV) 6. Levels of tau expression in the axons of *Tau*$^{-/-}$ neurons transfected with Tau-WT were comparable to those in untransfected *Tau*$^{+/+}$ neurons, although there was an increase in total tau (EP2456Y) in the soma, a slight decrease in phosphorylated (PHF-1) tau in the axon, and an increase in dephosphorylated (Tau-1) tau in the axon (Fig. 3, A–E). We then analyzed axonal mitochondrial motility in transfected neurons before and during application of recombinant $A\beta_{1-42}$ oligomers at DIV 7–8. Aβ impaired axonal transport in *Tau*$^{-/-}$ neurons expressing Tau-WT but not in *Tau*$^{-/-}$ neurons transfected with the empty plasmid (Fig. 3, F and G). At the expression levels used here, Tau-WT did not affect axonal transport in the absence of Aβ oligomers (Fig. 3 G).

Tau lacking the microtubule-binding region enables Aβ-induced axonal transport defects

To determine which domains of tau are most critical for Aβ-induced axonal transport deficits, we generated various tau truncation constructs derived from Tau-WT (Fig. 4 A) and transfected them into *Tau*$^{-/-}$ neurons. Protein expression by each construct was confirmed in transfected HEK293T cells by Western blot analysis (Fig. S3 A). When expressed in transfected *Tau*$^{-/-}$ neurons, the truncation constructs showed a similar distribution as the Tau-WT plasmid, indicating widespread intracellular distribution of each tau species (Fig. S3, B–G).

We assessed the relative microtubule binding within the axon for each transfected construct by the proximity ligation

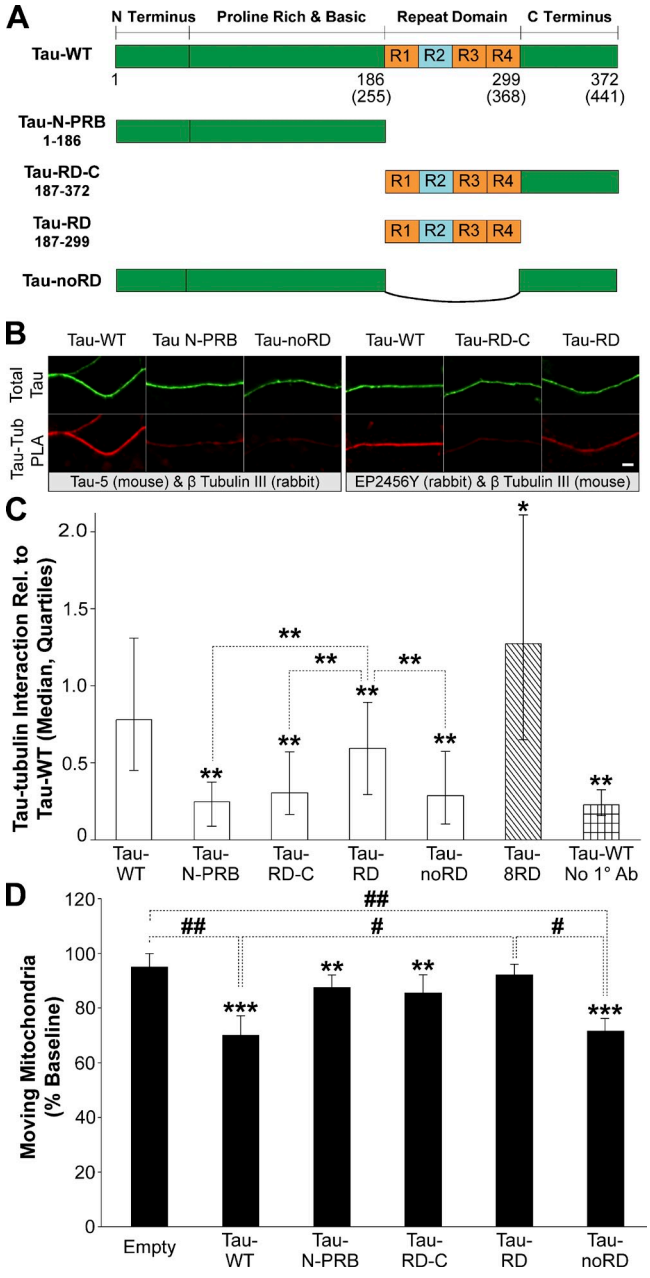

Figure 4. **Differential ability of tau truncation mutants to reconstitute susceptibility to Aβ-induced axonal transport deficits in *Tau*$^{-/-}$ neurons.** (A) Schematic of full-length Tau-WT and truncation constructs generated. N-PRB, N terminus plus proline-rich and basic domain; RD-C, repeat domain and C terminus; RD, repeat domain alone; noRD, tau lacking the repeat domain. Numbers indicate amino acid positions in mouse 0N4R tau and numbers in parentheses are the corresponding amino acid positions in human 2N4R tau. (B) In the axons of *Tau*$^{-/-}$ neurons transfected with plasmids encoding the indicated tau constructs, tau–tubulin binding was measured with the proximity ligation assay (PLA). Antibody combinations with source species in parentheses are indicated below each set of panels. Bar, 20 µm. (C) Quantification of the total proximity ligation assay signal (B, bottom), indicating the amount of tau that closely interacts with tubulin. A tau construct containing eight repeat domains (Tau-8RD), which has a higher tubulin binding affinity than wild-type tau (Preuss et al., 1997), was used as a positive control, and a no-primary tau antibody condition was used as a negative control. n = 37–256 axons per group. *, $P < 0.05$; **, $P < 0.01$ versus Tau-WT or for pairwise comparisons as indicated by brackets (Kruskal-Wallis ANOVA, Dunn's test). (D) The percentage of moving mitochondria in the axons of *Tau*$^{-/-}$ neurons transfected with empty plasmid or plasmids encoding the indicated tau constructs was measured before (baseline) and 10–60 min after adding $A\beta_{1-42}$ oligomers to the medium. Results are expressed relative to baseline (100%). n = 28–55 axons per construct recorded during three to five independent sessions at DIV 7–8 d. **, $P < 0.01$; ***, $P < 0.001$ versus corresponding baseline (paired t tests, Bonferroni); #, $P < 0.05$; ##, $P < 0.01$ (Kruskal-Wallis ANOVA, Dunn's test). Data in C are medians and quartiles, and data in D are means ± SEM.

assay, which detects interactions between proteins within a distance of 40 nm or less (Söderberg et al., 2006). Each of the truncation constructs showed lower levels of tubulin binding than Tau-WT when expressed in transfected *Tau*$^{-/-}$ neurons (Fig. 4, B and C), consistent with previous results for similar forms of truncated tau when expressed in Chinese hamster ovary cells (Preuss et al., 1997) or incubated with microtubule-containing cytosol from squid optic lobes (LaPointe et al., 2009). The tau repeat domain by itself (Tau-RD) showed higher levels of tubulin binding than the other truncation constructs (Fig. 4, B and C).

Surprisingly, tau lacking the repeat domain (Tau-noRD) was as effective as Tau-WT in enabling Aβ-induced axonal transport deficits in *Tau*$^{-/-}$ neurons, whereas the tau repeat domain by itself was ineffective (Fig. 4 D). Tau containing the N terminus and the proline-rich and basic region and tau containing the repeat domain and the C terminus also enabled Aβ-induced axonal transport deficits, but only to a modest degree that did not reach statistical significance when compared with the empty plasmid control (Fig. 4 D). At the expression levels used here, none of the tau constructs affected axonal transport in the absence of Aβ oligomers (Fig. S4 A). Because Tau-noRD has little affinity for microtubules (Fig. 4, B and C; Preuss et al., 1997; LaPointe et al., 2009), Tau-noRD likely enables Aβ-induced axonal transport deficits through a mechanism that is independent of microtubule binding.

Tau has been implicated in Aβ-induced cytoskeletal changes (King et al., 2006; Zempel et al., 2013), including deacetylation and polyglutamylation of tubulin and microtubule disassembly within dendrites of subpopulations of neurons (Zempel et al., 2010, 2013). However, Aβ treatment for 1 h did not alter acetylation or polyglutamylation of tubulin in *Tau*$^{+/+}$ or *Tau*$^{-/-}$ neurons (Fig. S5), further supporting a mechanism of Aβ/tau-dependent axonal transport deficits that is independent of tau–tubulin interactions.

Blocking neuronal activity abolishes Aβ-dependent deficits in axonal transport

Tau regulates neuronal excitability (Roberson et al., 2007; Ittner et al., 2010; Roberson et al., 2011; DeVos et al., 2013; Holth et al., 2013; Gheyara et al., 2014), and synaptic excitation can inhibit axonal transport of mitochondria (Lardong et al., 2009). Therefore, we assessed the effects of neuronal activity on Aβ-induced axonal transport deficits. Silencing the activity of *Tau*$^{+/+}$ neurons by treating them with tetrodotoxin (TTX) prevented Aβ-induced defects in axonal transport, but did not affect axonal transport in the absence of Aβ oligomers (Fig. 5 A).

Because acute rises in intracellular calcium ($[Ca^{2+}]_i$) can halt mitochondrial movements (Wang and Schwarz, 2009), we next assessed the effects of Aβ oligomers on neuronal calcium levels.

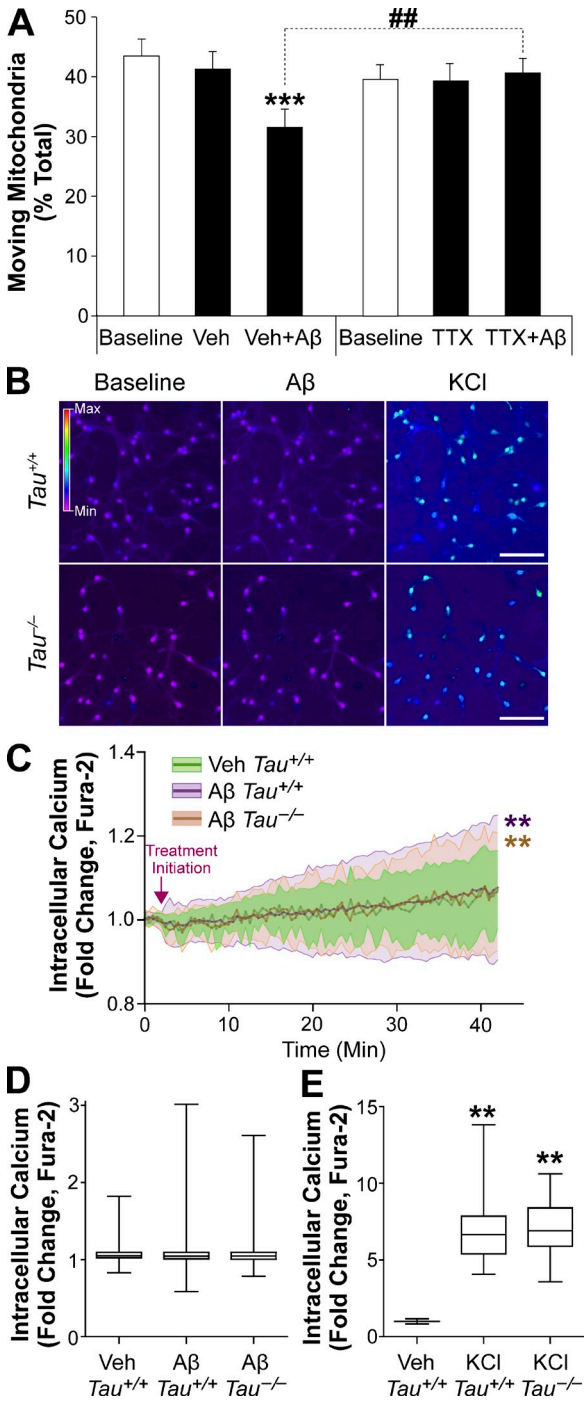

Figure 5. **Aβ-induced deficits in axonal transport depend on neuronal activity, but are not associated with obvious rises in $[Ca^{2+}]_i$.** (A) Primary hippocampal neurons from wild-type mice were treated with TTX (1 µM) to silence neuronal activity or with vehicle (Veh), followed by exposure to $Aβ_{1–42}$ oligomers. The percentage of moving mitochondria in the axons of $Tau^{+/+}$ neurons was measured before (baseline) and during these treatments. n = 22–26 axons per treatment combination from three independent sessions at DIV 12–14. ##, $P < 0.01$ as indicated by bracket (unpaired t test); ***, $P < 0.001$ versus corresponding baseline (repeated measures ANOVA, Dunnett's test). (B–E) $[Ca^{2+}]_i$ levels in primary hippocampal neurons from $Tau^{+/+}$ and $Tau^{-/-}$ mice were measured with Fura-2 (340:380 ratio) by live fluorescence microscopy at baseline (2 min) and after adding $Aβ_{1–42}$ oligomers (for 40 min) or KCl (50 mM final concentration for 5 min) to the medium. (B) Representative images of the cultures. Bars, 100 µm. (C–E) Quantitation of $[Ca^{2+}]_i$ relative to baseline levels (arbitrarily defined as 1.0). Aβ increased the variance in $[Ca^{2+}]_i$ in both genotypes compared with vehicle-treated $Tau^{+/+}$ neurons. **, $P < 0.01$ (Levene's test). Kruskal-Wallis ANOVA, followed by Dunn's post hoc test confirmed that the sevenfold rise in $[Ca^{2+}]_i$ induced by KCl in both genotypes was significant compared with vehicle-treated $Tau^{+/+}$ neurons (**, $P < 0.01$) and revealed no differences between genotypes for Aβ and KCl. (C and D) n = 356–1,002 neurons per genotype from 5–11 independent sessions at DIV 12–14. (E) n = 63–356 neurons per genotype from two to five independent sessions at DIV 12–14. Data in A are means ± SEM. Data in C are means ± SD. Plots in D and E show medians, quartiles, and ranges.

Exposure to Aβ oligomers for 40 min increased the variability in $[Ca^{2+}]_i$ levels in $Tau^{+/+}$ and $Tau^{-/-}$ neurons without causing a significant rise in $[Ca^{2+}]_i$ levels in either genotype (Fig. 5, B–D). Acutely depolarizing neurons with KCl induced marked rises in $[Ca^{2+}]_i$ that were similar in $Tau^{+/+}$ and $Tau^{-/-}$ neurons (Fig. 5, B and E), indicating that tau reduction does not grossly affect synaptic activity-induced $[Ca^{2+}]_i$ modulation. Thus, Aβ-induced deficits in the axonal transport of mitochondria require neuronal activity but do not likely involve large rises in $[Ca^{2+}]_i$.

Aβ-induced axonal transport deficits do not require tau–Fyn interactions

Aβ-induced axonal transport deficits depend on NMDAR function (Fig. 1 F; Decker et al., 2010; Tang et al., 2012), which can be modulated by the tyrosine kinase Fyn (Trepanier et al., 2012). Furthermore, tau has been implicated in NMDAR/Fyn-mediated excitotoxicity (Ittner et al., 2010), and reducing tau prevents aberrant neuronal excitation and cognitive deficits in hAPP/Fyn overexpressing mice (Roberson et al., 2011). To determine whether phosphorylation or binding of tau by Fyn are necessary for Aβ-induced axonal transport deficits, we generated a 0N4R mouse tau containing a tyrosine-to-phenylalanine substitution at residue 18 (Tau-Y18F), the major Fyn phosphorylation site of tau (Lee et al., 2004), and a 0N4R mouse Tau-AxxA7 construct with proline-to-alanine substitutions in the seventh proline-directed region of tau (PxxP → AxxA at amino acids 164–167 in mouse tau, corresponding to 233–236 in human 2N4R tau; Fig. 6 A), the major Fyn-binding site of tau (Lee et al., 1998).

We compared the effects of these constructs on axonal transport in $Tau^{-/-}$ neurons with those of Tau-WT and the empty plasmid under baseline conditions and in the presence of Aβ oligomers (Fig. 6 B). Both Tau-Y18F and Tau-AxxA7 enabled Aβ-induced axonal transport to a similar degree as Tau-WT, whereas the empty plasmid did not (Fig. 6 B). Neither Tau-Y18F nor Tau-AxxA7 affected axonal transport in the absence of Aβ oligomers (Fig. S4 B). These findings suggest that Fyn phosphorylation of tau and tau–Fyn binding are not necessary for tau to enable Aβ-induced axonal transport deficits.

Aβ-induced axonal transport deficits depend on GSK3β activation, which is prevented by tau ablation

Because GSK3β activity is required for Aβ-induced axonal transport deficits in several AD-related models (Rui et al., 2006; Decker et al., 2010; Tang et al., 2012), we next assessed the role of this kinase in our axonal transport assay. Treating wild-type

neuronal cultures with two distinct siRNAs targeting GSK3β or with the selective GSK-3 inhibitor SB 415286 (Coghlan et al., 2000; Cross et al., 2001) prevented Aβ-induced axonal transport deficits without affecting axonal transport in the absence of Aβ oligomers (Fig. 7). Remarkably, tau ablation prevented the Aβ-induced activation of GSK3β, which in wild-type neurons occurred within 30 min of adding Aβ oligomers to the medium (Fig. 8, A and B). Tau ablation did not affect total GSK3β levels (Fig. 8 C). These data support a role for tau in regulating Aβ-induced GSK3β activation, which is critical for Aβ-induced axonal transport deficits.

Discussion

Our study indicates that endogenous tau enables Aβ-induced deficits in mitochondrial axonal transport through a mechanism that is independent of its microtubule-binding capacity. Several additional factors were necessary for Aβ to impair axonal transport, including neuronal activity, NMDAR signaling, and GSK3β activity, and each of these critical elements can be influenced by tau, as demonstrated by this and previous studies (Roberson et al., 2007, 2011; Ittner et al., 2010; Miao et al., 2010; Kanaan et al., 2011; Leroy et al., 2012; DeVos et al., 2013; Holth et al., 2013; Gheyara et al., 2014). Notably, we found that tau enables Aβ-induced activation of GSK3β, an important kinase in AD pathogenesis that negatively regulates kinesin-based axonal transport (Morfini et al., 2002).

Similar to genetic tau ablation, postnatal tau knockdown also prevented Aβ-induced deficits in mitochondrial axonal transport, indicating that the mechanism by which tau ablation is protective against Aβ does not depend on compensatory developmental changes that may occur in *Tau*$^{-/-}$ mice. Because tau knockdown is well tolerated in adult mice (DeVos et al., 2013) and did not adversely affect mitochondrial motility in the current study, our findings provide further support for tau reduction as a viable therapeutic strategy for AD and related disorders (Roberson et al., 2007; Morris et al., 2011). Tau knockdown with siRNA oligonucleotides in cortical neurons also diminished mitochondrial fragmentation and motility deficits in a genetic model of spinocerebellar ataxia (SCA28) without affecting baseline mitochondrial morphology or transport, further highlighting the apparent safety and diverse indications for tau-reducing strategies (Kondadi et al., 2014).

Treating primary hippocampal neuronal cultures from hAPP-J20 mice with a potent GSM prevented deficits in anterograde mitochondrial transport. Such deficits were also observed in cultured neurons from hAPP transgenic mice of line Tg2576 (Calkins and Reddy, 2011) and could be prevented with γ-secretase inhibitors (Wang et al., 2012). Collectively, these findings highlight the importance of $A\beta_{1-42}$, which has a high propensity to oligomerize, for axonal transport impairments relative to other hAPP cleavage products and indicate that the Aβ-dependent axonal transport impairments are not restricted to one hAPP transgenic line.

We made several additional mechanistic observations that merit further discussion. The observation that Aβ-induced deficits in axonal transport occurred in tau-expressing neurons

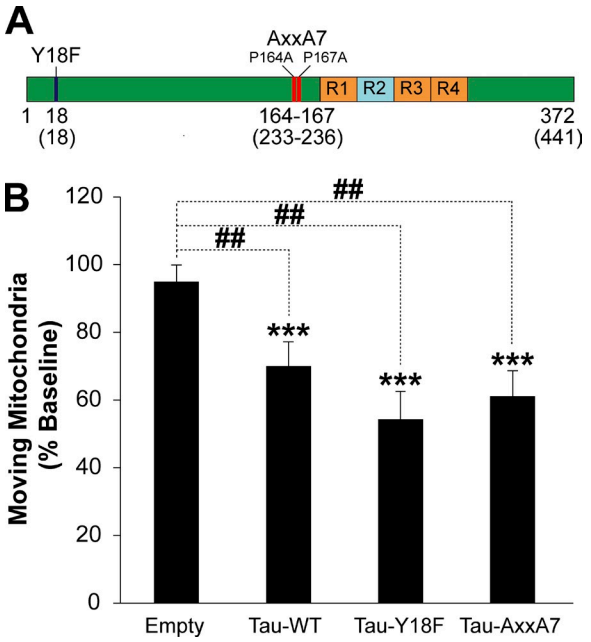

Figure 6. **Aβ-induced deficits in axonal transport do not depend on interactions between tau and Fyn.** (A) Diagram of 0N4R mouse tau indicating the Y18F point mutation that should prevent phosphorylation of tau by Fyn (Lee et al., 2004) and the PxxP to AxxA substitutions in the seventh proline-directed region (AxxA7) that should interfere with binding of tau to Fyn (Lee et al., 1998). Numbers in parentheses indicate corresponding amino acid positions in human 2N4R tau. (B) The percentage of moving mitochondria in the axons of *Tau*$^{-/-}$ neurons transfected with empty plasmid or plasmids encoding the indicated tau constructs was measured before (baseline) and 10–60 min after adding $A\beta_{1-42}$ oligomers to the medium. Results are expressed relative to baseline (100%). n = 19–37 axons per construct recorded during three to five independent sessions at DIV 7–8. ##, $P < 0.01$ versus empty (Kruskal-Wallis ANOVA, Dunn's test); ***, $P < 0.001$ versus corresponding baseline (paired t tests, Bonferroni). Data are means ± SEM.

added in small numbers to cultures of *Tau*$^{-/-}$ neurons suggests a cell autonomous mechanism for tau's enabling effect. Conceivably, tau may enable Aβ-dependent transport deficits locally within the axon and through distal mechanisms in dendrites or presynaptic terminals. Indeed, we observed that endogenous tau can be readily detected in cell bodies and dendrites of wild-type neurons cultured under standard conditions (Fig. 3 A), and others have shown that tau enables Aβ-induced deficits in mitochondrial motility also in dendrites (Zempel et al., 2013). Pharmacological inhibition of NMDARs (AP5), which are concentrated at postsynaptic sites, and silencing neuronal activity (TTX), which prevents presynaptic action potential–driven neurotransmitter release, prevented Aβ-induced deficits in mitochondrial axonal transport, highlighting the multifactorial nature of this pathogenic process. AP5 and TTX also prevented Aβ-induced increases in DNA double-strand breaks, which also depend on tau (Suberbielle et al., 2013).

Aβ may perturb NMDAR signaling through a number of possible mechanisms, including the following: (a) directly or indirectly activating NMDARs (Kelly and Ferreira, 2006; De Felice et al., 2007), (b) altering the intrasynaptic–extrasynaptic balance by causing internalization of synaptic NMDAR through long-term depression-like mechanisms (Li et al., 2009) or binding to EphB2 (Cissé et al., 2011), and (c) activating a metabotropic

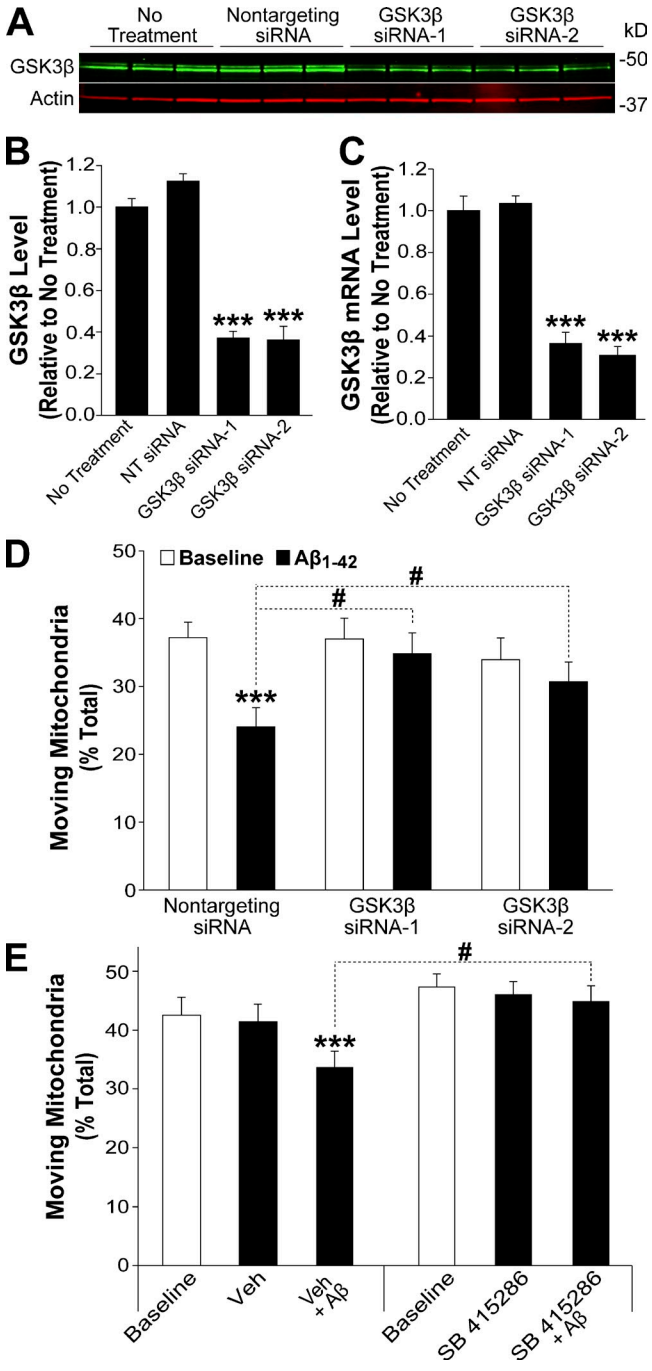

Figure 7. **Aβ-induced deficits in axonal transport depend on GSK3β.** (A–C) On DIV 10, neuronal cultures from wild-type mice were treated with nontargeting (NT) siRNA or siRNAs (siRNA-1 or siRNA-2) targeting GSK3β mRNA. GSK3β protein levels were determined by Western blotting on DIV 14. (A) Representative Western blot from a single gel that was scanned and digitally arranged. (B) Quantitation of Western blot signals. (C) mRNA levels were determined by RT-qPCR in replicate cultures on DIV 13. n = 3–12 samples per condition. ***, $P < 0.001$ versus no treatment (Dunnett's test). (D) Primary hippocampal neurons from wild-type mice were treated with NT siRNA or anti-GSK3β siRNA on DIV 9–10. On DIV 13–14, the percentage of moving mitochondria in the axons was measured before (baseline) and during treatment with $A\beta_{1-42}$. n = 20–27 axons per group from three to four independent sessions. #, $P < 0.05$ (Kruskal-Wallis ANOVA, Dunn's test); ***, $P < 0.001$ versus corresponding baseline (paired t test, Bonferroni). (E) Primary hippocampal neurons from wild-type mice were treated with the selective GSK-3 inhibitor SB 415286 (10 µM) or vehicle (Veh), followed by exposure to $A\beta_{1-42}$ oligomers. The percentage of moving mitochondria in the axons of *Tau*$^{+/+}$ neurons was measured before (baseline) and during these treatments. n = 23–27 axons per group from four independent sessions at DIV 13–14. #, $P < 0.01$ (Mann-Whitney rank-sum test); ***, $P < 0.001$ versus corresponding baseline (repeated measures ANOVA, Dunnett's test). Data are means ± SEM.

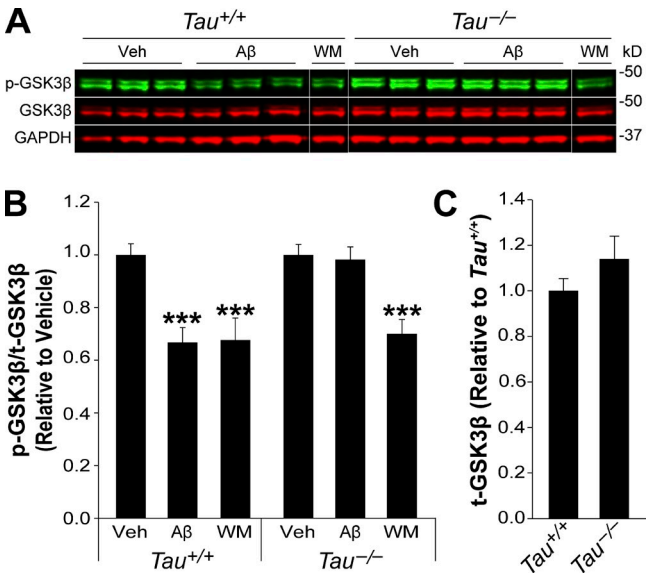

Figure 8. **Tau reduction prevents Aβ-induced activation of GSK3β.** (A–C) Phosphorylation of GSK3β at serine 9 (p-GSK3β), a modification that inhibits GSK3β activity (Sutherland et al., 1993), and total GSK3β (t-GSK3β) and GAPDH or actin levels in *Tau*$^{+/+}$ and *Tau*$^{-/-}$ neurons were determined by Western blot analysis after treatment of neuronal cultures with vehicle (Veh), $A\beta_{1-42}$ oligomers (30 min), or the phosphoinositide 3-kinase inhibitor wortmannin (WM; 0.1 µM, 30 min). (A) Representative Western blot from a single gel that was scanned and digitally arranged. (B) Quantitation of the p-GSK3β/t-GSK3β ratio for each treatment. Aβ decreased the ratio (i.e., increased GSK3β activity) in *Tau*$^{+/+}$, but not *Tau*$^{-/-}$, neurons, whereas WM decreased the ratio in both types of neurons. (C) Quantitation of t-GSK3β levels revealed no significant difference between vehicle-treated *Tau*$^{+/+}$ and *Tau*$^{-/-}$ neurons (t test). n = 7–18 wells per condition from three to six independent experiments at DIV 14. ***, $P < 0.001$ versus vehicle in the same genotype (Dunnett's test). Data are means ± SEM.

function of NMDAR that is independent of calcium influx (Kessels et al., 2013).

To study the influence of tau on NMDAR-associated cell signaling, we studied two relevant kinases, Fyn and GSK3β. Although tau–Fyn interactions appear to be primarily pathogenic in AD models (Ittner et al., 2010; Seward et al., 2013), Fyn phosphorylation of tau at Y18 prevented anterograde axonal transport deficits caused by filamentous tau and the 6D isoform of tau, most likely by inhibiting the N-terminal phosphatase-activating domain of tau (Kanaan et al., 2012). Therefore, inhibiting Fyn phosphorylation of tau in the axon could, in principle, be deleterious. However, we found that preventing Fyn phosphorylation of tau at tyrosine 18 or tau–Fyn binding through tau mutagenesis did not affect baseline transport; nor did it prevent Aβ-induced axonal transport deficits. Additional studies are needed to determine whether tau enables Aβ-induced axonal transport deficits by affecting NMDAR signaling through a Fyn-independent mechanism or by processes that occur downstream of or in parallel to NMDAR functions.

In regards to GSK3β, much attention has focused on potential deleterious effects of tau that is phosphorylated by GSK3β (Augustinack et al., 2002; Terwel et al., 2008). Our findings suggest that endogenous tau in turn regulates GSK3β activity, consistent with findings obtained in models of heat shock–induced neuronal injury and in mutant APP/presenilin 1 (PS1) transgenic mice. $Tau^{-/-}$ neurons showed less GSK3β activity than $Tau^{+/+}$ neurons during recovery from heat shock (Miao et al., 2010), and APP/PS1/$Tau^{-/-}$ mice had lower levels of active GSK3β in the brain than APP/PS1/$Tau^{+/+}$ mice (Leroy et al., 2012).

Tau may influence GSK3β through numerous pathways including PI3K–Akt (Takashima et al., 1996), protein phosphatase 1 (Kanaan et al., 2011), caspase-3–Akt (Jo et al., 2011), calcineurin (Snyder et al., 2005), and Wnt signaling (Caricasole et al., 2004). Tau interacts with many of these relevant kinases that are upstream of GSK3β (Morris et al., 2011) and with GSK3β itself (Agarwal-Mawal et al., 2003; Sun et al., 2002). Interestingly, 3,4-methylenedioxymethamphetamine also impairs axonal mitochondrial transport by a tau- and GSK3β-dependent mechanism (Barbosa et al., 2014), indicating that tau reduction may be protective against other neurotoxins involving GSK3β signaling. Tau reduction also prevents Aβ-induced deficits in hippocampal long-term potentiation (Roberson et al., 2011; Shipton et al., 2011), but reduces hippocampal long-term depression (Kimura et al., 2014). Conceivably, effects of endogenous tau on GSK3β, a key regulator of long-term potentiation and depression (Peineau et al., 2007; Jo et al., 2011), may account for these observations.

In addition to GSK3β, there may be other disease-relevant signaling molecules that regulate axonal transport and depend on tau. It is interesting in this regard that Tau-noRD enabled Aβ-induced axonal transport deficits more effectively than tau containing the N terminus and the proline-rich and basic region and tau containing the repeat domain and the C terminus (Fig. 4). Conceivably, tau that is not bound to microtubules might act as an organizer of signaling microdomains, assembling relevant binding partners through domains preserved in Tau-noRD. Indeed, tau has a growing list of binding partners that are known to participate in diverse functions (Morris et al., 2011).

Additional studies are needed to further dissect these and other relevant cell signaling pathways and to address some of the limitations of this study, including the following caveats. First, we studied general patterns of mitochondrial motility, velocity, and length. Although these measures yielded robust and informative findings, they did not comprehensively characterize all aspects of mitochondrial dynamics, such as brief pausing or fission/fusion events.

Second, we focused on a relatively short time window of Aβ exposure and on a single cargo. Others have shown that Aβ-induced deficits of brain-derived neurotrophic factor axonal transport, which are observed after 18–72 h of Aβ exposure, are independent of tau (Ramser et al., 2013). Thus, it is conceivable that effects of Aβ on other cargoes or at later time points may not depend on tau.

Third, although we found no Aβ-induced rises in overall neuronal calcium levels or changes in indicators of tubulin stability during the timeframe in which Aβ impaired axonal mitochondrial transport, we cannot rule out more subtle effects of Aβ or tau on these factors that may be below the detection threshold of the methods used here. A recent study indicates that Aβ can increase neuronal calcium levels through effects on neighboring astrocytes (Talantova et al., 2013). Our use of the glial inhibitor 5-Fdu and neurobasal medium, which selects for neurons in culture (Sanchez-Mejia et al., 2008), could explain why we did not observe an overall increase in $[Ca^{2+}]_i$ after Aβ application. We did, however, find a significantly increased variability in $[Ca^{2+}]_i$ levels after Aβ application as compared with vehicle (Fig. 5 C), consistent with subpopulations of hyperactive (higher calcium levels) and hypoactive (lower calcium levels) neurons without overall increases in $[Ca^{2+}]_i$ observed by others (Busche et al., 2008; Renner et al., 2010).

In a previous study, Aβ did not affect microtubule integrity in axons, even in the subpopulations of neurons that showed increased $[Ca^{2+}]_i$ levels and dendritic changes in microtubule density (Zempel et al., 2013). Axonal microtubules, which are tightly packed, are particularly resistant to depolymerization induced by Ca^{2+} and other destabilizing treatments (Brady et al., 1984; Song et al., 2013). Additionally, others have shown that eliminating Ca^{2+} influx or buffering $[Ca^{2+}]_i$ within neurites did not prevent Aβ-induced deficits in mitochondrial transport (Rui et al., 2006). Therefore, we consider it unlikely that Aβ-induced alterations in $[Ca^{2+}]_i$ or changes in microtubule stability in small subpopulations of neurons caused the global effect of Aβ on mitochondrial transport in the population of axons we analyzed.

Fourth, we did not study tau's potential role in actin polymerization, which also appears to be involved in Aβ-induced axonal transport deficits (Hiruma et al., 2003). However, tau's repeat domain, which is important for actin binding and bundling (Yu and Rasenick, 2006; He et al., 2009), did not, by itself, enable Aβ-induced axonal transport deficits in the current study, whereas tau lacking this domain did. These findings would seem to make a prominent role of actin modulation in the deficit-enabling role of tau less likely.

Fifth, the relevance of our findings to axonal transport in the mature or aging brain remains to be determined. Advances in technology are likely needed to measure mitochondrial axonal transport in hippocampal neurons within the living adult brain. Notably, global axonal transport deficits have been shown to impair long-term potentiation (Barnes et al., 2010) and learning and memory (Nakayama and Sawada, 2002), and even modest reductions in axonal mitochondrial transport can cause profound neurological deficits in mice (Nguyen et al., 2014).

Sixth, we acknowledge that different Aβ oligomer preparations can have variable potency and biological activity. Importantly, in every experiment in which tau or signaling pathways were manipulated, experimental and control cultures were exposed to the same $Aβ_{1–42}$ preparation, making it unlikely that variations in the biological activity of $Aβ_{1–42}$ preparations confounded the interpretation of our key findings.

In summary, we have shown that Aβ oligomers acutely impair axonal transport of mitochondria in a tau-dependent manner through a mechanism that is independent of tau's microtubule-binding domain and of developmental changes that

may occur in neurons of *Tau*$^{-/-}$ mice. These findings add to growing evidence that endogenous tau regulates disease-relevant neuronal functions in a microtubule-independent fashion (Reynolds et al., 2008; Leugers and Lee, 2010; Morris et al., 2011). Our tau-reconstitution assay provides a new approach to further study mechanisms underlying Aβ- and tau-dependent neuronal deficits, including the intriguing mediator role that GSK3β appears to have in this process.

Materials and methods

Plasmid constructs

The plasmid backbone for all tau constructs was FUGW (provided by L. Gan, Gladstone Institute of Neurological Disease, San Francisco, CA), which contains a ubiquitin C promoter (Lois et al., 2002). Each tau insert replaced the EGFP sequence within FUGW between the AscI and RsrII restriction enzyme sites. The tau sequence was based on the most abundant isoform of mouse wild-type tau in mature neurons, 0N4R, which is 372 amino acids in length (McMillan et al., 2008; Peruzzi et al., 2009). The structure of the tau truncation constructs is shown in Fig. 4 A, with equivalent amino acids in the human 2N4R 441-residue isoform (NCBI Protein database accession no. NP_005901.2) shown in parentheses. Tau truncation constructs were created through PCR amplification of segments of Tau-WT. The tyrosine-to-phenylalanine mutation at residue 18 (Y18F) and the proline-to-alanine mutations at residues 164 and 167 (AxxA7) were introduced into the Tau-WT sequence using the QuikChange II XL site-directed mutagenesis kit (Agilent Technologies). All plasmid sequences were verified by DNA sequencing. The mito-RFP construct, which labels mitochondria with RFP (Yoon et al., 2003), was provided by Y. Yoon (Georgia Regents University, Augusta, GA). Mito-RFP was constructed by fusing the mitochondrial targeting sequence of human isovaleryl coenzyme A dehydrogenase to the N terminus of RFP within the pDsRed1-N1 vector backbone, which contains a CMV promoter (Takara Bio Inc.; Yoon et al., 2003).

Mice, primary neuronal cultures, and transfections

Tau$^{-/-}$ mice, which were generated by homologous recombination replacing exon 1 of the *Tau* gene with a neomycin resistance cassette (Dawson et al., 2001), were obtained from H.N. Dawson and M.P. Vitek (Duke University, Durham, NC). *Tau*$^{+/-}$ and hAPP/*Tau*$^{+/-}$ mice were generated by breeding *Tau*$^{+/+}$ (C57Bl/6J strain; The Jackson Laboratory) and hAPP/*Tau*$^{+/+}$ mice from line J20, which expresses an hAPP minigene with the Swedish (K670M/N671L) and Indiana (V717F) familial AD mutations directed by the platelet-derived growth factor promoter (Mucke et al., 2000), with *Tau*$^{-/-}$ mice. Littermates of six genotypes (*Tau*$^{+/+}$, *Tau*$^{+/-}$, *Tau*$^{-/-}$, hAPP/*Tau*$^{+/+}$, hAPP/*Tau*$^{+/-}$, and hAPP/*Tau*$^{-/-}$) were generated by breeding *Tau*$^{+/-}$ mice with hAPP/*Tau*$^{+/-}$ mice. *Tau*$^{+/+}$, *Tau*$^{+/-}$, and *Tau*$^{-/-}$ littermates were also generated by breeding *Tau*$^{+/+}$, *Tau*$^{+/-}$, or *Tau*$^{-/-}$ with each other. *Tau*$^{-/-}$ mice were not bred with each other for more than one generation. Primary neuronal cultures were established using postnatal day 0 pups. Hippocampal and cortical regions were dissected in cold Earle's balanced salt solution (Gibco) and digested with 10 U/ml papain (Worthington Biochemical Corporation) in Earle's balanced salt solution for 15 min at 37°C. Low ovomucoid solution containing 0.15% BSA (Sigma-Aldrich), 0.15% trypsin inhibitor (Sigma-Aldrich) in Dulbecco's phosphate-buffered saline (DPBS) with calcium and magnesium (Gibco), and 66.6 U/ml deoxyribonuclease I (Sigma-Aldrich) was added to stop the digestion reaction. After 5 min, the cells were suspended in fresh low ovomucoid solution. Debris was removed with a 70-µm nylon strainer (BD), and the cells were spun at 1,000 rpm for 10 min. Cell pellets were then resuspended in warm Neurobasal A medium (Gibco), containing 2% B27 (Gibco), 0.5 mM GlutaMAX (Gibco), and 100 U/ml penicillin/streptomycin (Gibco). Cortical and mixed hippocampal and cortical cells underwent an additional step to remove debris: the cell suspension was filtered through 4% BSA dissolved in neurobasal A by centrifugation at 1,000 rpm for 10 min. The cells were then resuspended in warm medium.

Hippocampal primary neurons were plated on glass-bottom microwell dishes (MatTek Corporation) that had been coated overnight with 0.5 mg/ml poly-L-lysine (Sigma-Aldrich) in borate buffer and for 1–2 h with 0.005 mg/ml laminin (Roche) in neurobasal A. Hippocampal cells were seeded at a density of 400,000 cells per 10-mm microwell dish for axonal transport experiments and immunocytochemistry and of 270,000 cells per dish for calcium imaging. Cortical primary neurons were plated on multiwell flat-bottom plates that had been coated with 0.05 mg/ml poly-D-lysine (EMD Millipore) in water for at least 3 h. Cortical cells were seeded at a density of 1.5 million cells per well on 12-well plates (Falcon) or 0.75 million cells per well on 24-well plates (Falcon). Mixed cortical and hippocampal neurons were plated on 96-well plates that were precoated with poly-D-lysine (CELLCOAT) at a density of 80,000 cells per well. For 96-well plates, N2 supplement (Gibco) was added to the medium at a dilution of 1:100 to maintain healthy cultures. After 24 h, 5-fluoro-2′-deoxyuridine (Sigma-Aldrich) was added at a final concentration of 7.15 µg/ml to inhibit glial growth. Half-medium changes were performed every 7 d to maintain culture health.

Transient transfections of hippocampal neuronal cultures were performed on DIV 6. After the removal of conditioned medium, cells were washed once with warm DPBS without calcium or magnesium (Gibco) and immediately placed into warm transfection medium (500 µl per dish) consisting of Neurobasal A (Gibco) with 0.5 mM GlutaMAX (Gibco), 1 mM kynurenic acid (Sigma-Aldrich), and 10 mM magnesium chloride (Sigma-Aldrich) for at least 30 min. To prepare the transfection complexes, Lipofectamine 2000 (Invitrogen) was added to OptiMEM reduced serum medium with GlutaMAX (Gibco) at a ratio of 1.35 µl Lipofectamine per 25 µl OptiMEM. In separate tubes, plasmid DNA was combined in amounts that were equimolar to 1 µg FUGW per 25 ml OptiMEM. After incubating separately for 5 min, the Lipofectamine-OptiMEM and DNA-OptiMEM solutions were combined and incubated at room temperature while covered for 25 min. Then, 50 ml of combined transfection solution was added to each microwell dish. After the addition of the transfection solutions, the neuronal cultures were incubated for 30 min at 37°C. Finally, the cells were washed twice with warm DPBS and immediately placed into 3/4 conditioned medium and 1/4 fresh medium. For tau reconstitution experiments, tau constructs were cotransfected into *Tau*$^{-/-}$ neurons with FUGW and mito-RFP in 1:1:1 molar ratios. We verified by immunocytochemistry of fixed cells from three independent cultures that all neurons transfected with FUGW and mito-RFP also expressed the tau construct, as shown in Fig. 3 F.

ELISA analysis of Aβ levels

Culture medium was collected at DIV 14 and analyzed by ELISA for levels of human $A\beta_{1\text{-}x}$ and $A\beta_{1\text{–}42}$ as described previously (Johnson-Wood et al., 1997). Medium was diluted 1:50 to measure $A\beta_{1\text{-}x}$ and 1:5 to measure $A\beta_{1\text{–}42}$ in this assay.

Lentiviruses expressing shRNA

Lentiviral vectors used for expression of shRNAs were based on FUGW (Lois et al., 2002) and were provided by J.A. Harris (Gladstone Institute of Neurological Disease, San Francisco, CA). Tau expression was reduced with shRNA targeting mouse tau placed under control of the U6 promoter. The target sequence for the anti-tau shRNA was 5′-ACAGAGTCCAGTCGAAGATT-3′. The U6-shRNA expression cassette (pSilencer 2.0; Ambion) was inserted between the NheI and PacI sites of a modified FUGW lentiviral backbone, placing the U6-shRNA cassette upstream of a ubiquitin C promoter directing expression of EGFP. A similar construct expressing a scrambled shRNA (sequence 5′-CCACTACCGTTGTTATAGGTG-3′) was used as a control. Active lentiviral particles were generated by cotransfecting the transfer vector with two helper plasmids, delta 8.9 (packaging vector) and VSV-G (envelope vector), into HEK293T cells. The transfected HEK293T cells were placed in an incubator at 3% CO_2 and 37°C overnight, and then at 10% CO_2 and 37°C for 2 d. Medium was collected once daily during the last 2 d and filtered through a 0.22-µm filter. The medium was then loaded in SW28 tubes (Beckman Coulter) and centrifuged at 21,000 rpm (50,000 *g*) for 2 h in an ultracentrifuge at room temperature. Pellets from 10 ml of medium each were resuspended in HBSS (Gibco) using 1 ml HBSS per pellet. Pooled particles were loaded in a volume of 2.5 ml on 2 ml 20% sucrose (in HBSS) in SW55 tubes (Beckman Coulter) and centrifuged at 25,000 rpm (50,000 *g*) for 2 h in an ultracentrifuge at room temperature. Each pellet was resuspended in 100 µl HBSS and viral particles were transferred into microcentrifuge tubes, shaken on vortex at low speed for 1 h at room temperature, quick-spun for 15 s, and then aliquoted and stored at −80°C. The viral titer (transducing units per milliliter) was determined by transducing HEK293T cells with tenfold serial viral dilutions and counting EGFP-expressing cells for each viral dilution. For transduction with lentivirus-shRNA constructs, neuronal cultures were infected with lentivirus at a multiplicity of infection of 2. Transduction of imaged neurons was confirmed by viewing EGFP.

Preparation of $A\beta_{1-42}$ oligomers

24 h before treatments, recombinant $A\beta_{1-42}$ peptide in hydroxyfluroisopropanol (rPeptide) was dissolved in DMSO (Sigma-Aldrich) to a concentration of 5 mM and then diluted in cold sterile-filtered PBS to 0.5 mg/ml. The Aβ was then incubated at 4°C without shaking overnight. This technique yields oligomeric species of $A\beta_{1-42}$ (Cheng et al., 2009). Synthetic $A\beta_{1-42}$ peptide (Biopeptide), prepared according to the same protocol with the added initial step of lyophilizing the peptide in hydroxyfluroisopropanol (Sigma-Aldrich), was used for some of the experiments in Fig. 5 and Fig. 8 (A and B). On Western blots, the rPeptide $A\beta_{1-42}$ preparation existed as low-order oligomers and the Biopeptide $A\beta_{1-42}$ preparation existed primarily as dimers (Fig. S2 C). By atomic force microscopy, both $A\beta_{1-42}$ preparations consisted of small globular aggregates, confirming their oligomeric state (Fig. S2 D). Freshly prepared Aβ was used for most experiments. In some experiments, we used Aβ preparations that had been snap-frozen and thawed. Except for the addition of Aβ, vehicle was prepared according to the same protocol. The Aβ concentration (monomeric equivalent) was measured on the day of the treatment using the Coomassie (Thermo Fisher Scientific) protein assay with BSA (Thermo Fisher Scientific) standard curve. The following formula was used to calculate the molar concentration of Aβ: Aβ concentration (M) = [sample concentration (μg/ml) × 10^{-6} g/μg × 1,000 ml/l]/4514.1 g/mol.

The concentrations of typical Aβ preparations were between 50 and 70 μM, and these preparations were diluted to a final concentration of 2 μM in the medium for culture treatments. To ensure the Aβ oligomer preparations were biologically active, each lot of Aβ oligomers was tested for its ability to increase phosphorylation of ERK1/2 within 30 min of addition to cortical neuronal cultures following an established protocol (Suberbielle et al., 2013). In this assay, 1 μM phorbol 12-myristate 13-acetate (Sigma-Aldrich), a phorbol ester that causes ERK1/2 phosphorylation by activating protein kinase C, was used as a positive control. Antibodies used for Western blot analysis of cell lysates were anti-phopho-ERK1/2 (rabbit; Cell Signaling Technology) at a dilution of 1:1,000 and anti-total ERK1/2 (mouse; Cell Signaling Technology) at a dilution of 1:2,000.

Culture treatments

Primary cortical neuronal cultures underwent treatments on DIV 14 for Western blot analyses (Figs. 8 and S5). To ensure equivalent neuronal activity levels across all wells, synaptic activity was first inhibited using a 3-h treatment with 10 μM NBQX (Santa Cruz Biotechnology, Inc.) and 100 μM D-AP5 (Tocris Bioscience) in conditioned medium. The cells were then washed twice with warm DPBS (Gibco) and immediately placed into conditioned medium at 37°C for ∼1 h before treatments.

Cells were treated with 2 μM Aβ, 0.1 μM wortmannin (Sigma-Aldrich), or 10 μg/ml nocodazole (Sigma-Aldrich) in conditioned medium or an equivalent amount of vehicle for 30 min or 1 h at 37°C. Immediately afterwards, the cells were washed once with warm DPBS and lysed with cold RIPA buffer consisting of 150 mM sodium chloride, 1% NP-40, 0.5% deoxycholic acid, 0.1% SDS, and 50 mM Tris, pH 7.4, and protease and phosphatase inhibitor cocktail (Thermo Fisher Scientific). Cell lysates were collected in Eppendorf tubes, sonicated for 5 min twice, centrifuged at 10,000 rpm for 10 min at 4°C, and stored at −20°C until protein analysis was performed.

The GSM (BMS-893204; $A\beta_{1-42}$ IC_{50} = 2 nM) was provided by D.S. Zuev, L.A. Thompson, and J.H. Toyn (Bristol-Myers Squibb, Wallingford, CT). The compound is (*S*)-*N*2-(4-(4-chloro-1*H*-imidazol-1-yl)-3-methoxyphenyl)-*N*4-methyl-7-phenyl-6,7-dihydro-5*H*-cyclopenta[d]pyrimidine-2,4-diamine and was prepared as reported previously (Boy et al., 2013). The compound was dissolved in DMSO to a stock concentration of 10 mM. For GSM treatment, BMS-893204 (100 nM, final concentration) was added to the medium of cultures on DIV 1 and 7. BMS-893204 concentrations ranging from 0.01 to 300 nM were tested for their ability to reduce $A\beta_{1-42}$ by >50% in culture medium from hAPP-J20 neurons, and 100 nM was determined to be the minimal effective concentration. A γ-secretase inhibitor (avagacestat [BMS-708163], $A\beta_{1-42}$ IC50 = 0.3 to 6.7 nM; Albright et al., 2013) was provided by Bristol-Myers Squibb and used as a positive control for Fig. S2 A. The γ-secretase inhibitor was dissolved in DMSO to a stock concentration of 10 mM and then added to the culture medium (100 nM, final concentration) at DIV 1 and 7.

The siRNAs targeting the 3′ untranslated region of mouse GSK3β and nontargeting control siRNA were obtained from the Mouse Accell siRNA Library (GE Healthcare) and resuspended in siRNA buffer (GE Healthcare) according to the manufacturer's instructions. The target sequences of the siRNAs and the nontargeting control siRNA used in this study are as follows: siRNA-1: 5′-CUCUUAUCCAAGUGAGAUC-3′; siRNA-2: 5′-GUGCUUGCCUGUAAAAUUU-3′; nontargeting siRNA, 5′-UGGUUUACAUGUUGUGUGA-3′.

Individual siRNAs were added to the culture medium of primary cortical and hippocampal neuronal cultures at DIV 10 (1 μM, final concentration), followed by measurements of GSK3β mRNA levels by reverse transcription-quantitative PCR (RT-qPCR) on DIV 13 and of GSK3β protein levels by Western blotting on DIV 14 in replicate cultures. In pilot experiments, we determined that 1 μM of an anti-GSK3β siRNA SMARTpool was the optimal dose to achieve >50% reduction in mRNA and protein without affecting cell viability after 4 d (alamarBlue assay). The nontargeting control siRNA also did not affect cell viability at this dose. We then tested each of the individual anti-GSK3β siRNAs from the SMARTpool (n = 4) and determined that two siRNAs were highly effective at silencing GSK3β expression without affecting cell viability at the 1 μM dose.

Immunocytochemistry, proximity ligation assay, and imaging

Neuronal cell cultures were fixed on DIV 7 (12–18 h after transfections) or 14 (nontransfected cultures) by 20-min incubation in warm 4% paraformaldehyde (Electron Microscopy Sciences) diluted in PBS (Teknova) in EMD Millipore water. Note that all washes were done with 0.01% Triton X-100 (Sigma-Aldrich) in PBS and that all of the following steps were conducted at room temperature on a shaker unless stated otherwise. After a 5-min wash, cells were permeabilized with 0.1% Triton X-100 in PBS for 10 min. The dishes were washed again for 5 min and then blocked with 10% donkey serum (Jackson ImmunoResearch Laboratories) in 0.01% Triton X-100 in PBS for 30 min. Cells were incubated on a shaker overnight at 4°C in primary antibodies (Table S1) diluted in PBS containing 10% donkey serum and 0.1% Triton X-100. The next day, cells were washed three times for 5 min and incubated for 1–5 h (incubation times: EP2456Y tau imaged in far red, 5 h; EP2456Y tau imaged in green, 1 h; Tau-5 imaged in green, 4 h; Tau-1 imaged in green, 1 h) in secondary antibodies (Table S2) diluted in PBS containing 10% donkey serum and 0.01% Triton X-100. After three 5-min washes, cell nuclei were counterstained with DAPI using VECTASHIELD Mounting Medium (Vector Laboratories). After three more 5-min washes, the cells were placed in PBS at 4°C until imaging.

Proximity ligation assays were performed on primary hippocampal cell cultures that were fixed on DIV 7 (1 d after transfections), permeabilized, and blocked as in the previous paragraph. The cultures were incubated on a shaker overnight at 4°C in primary antibodies (Table S1) that were diluted in 10% donkey serum in 0.1% Triton X-100 in PBS. The next day, the cells were washed three times for 5 min and then incubated for 1 h in DuoLink In-Situ Probes (Olink Bioscience; Table S2) prepared according to the manufacturer's directions. The incubation steps for the DuoLink In-Situ Probes (secondary antibodies), ligation, and amplification reactions were performed in a 37°C humidified incubator. Each secondary antibody was coupled with a plus or minus oligonucleotide sequence that interacted with each other when within 40-nm proximity. After two 5-min washes with wash buffer A (Olink Bioscience), the two nucleotide sequences were ligated for 1 h with a ligase prepared in a ligase buffer according to the manufacturer's directions and washed twice for 2 min with wash buffer A. Next, the sequences were amplified for 100 min using rolling circle amplification with a polymerase prepared in an amplification buffer according to the manufacturer's directions. The amplification buffer contained fluorophore-labeled oligonucleotide probes that hybridized to the amplification product, thereby allowing detection. The ligase, polymerase, ligation, and amplification buffers were part of the Duolink II Detection Reagents Red kit (Olink Bioscience). After amplification, the cells were washed twice for 10 min with wash buffer B (Olink Bioscience), washed once with 1% wash buffer B in PBS, and placed into PBS until imaging.

Images were acquired on a widefield epifluorescence system, consisting of a Ti-E microscope (Nikon) with a xenon arc lamp (Lambda LS; Sutter Instrument), motorized stage (Nikon), Coolsnap HQ2 CCD camera (Photometrics), 10× objective (Plan Apochromat, NA 0.45; Nikon), and NIS-Elements 4.2 acquisition software (Nikon). Excitation and emission filters were selected according to the fluorophores listed in Table S2. Excitation wavelengths were 485 nm to illuminate Alexa Fluor 488, 572 nm to illuminate Alexa Fluor 594 and Duolink II Detection Reagents Red, and 650 nm to illuminate Alexa Fluor 647. Images were also acquired on a spinning disk confocal unit (CSU-X M1; Yokogawa Electric Corporation) on an inverted microscope (TI 2000; Nikon) with an electron multiplying charge coupled device camera camera (Hamamatsu), 20× objective (Plan Apochromat, NA 0.75; Nikon), and open source MicroManager v1.4 acquisition software. Fluorophores listed in Table S2 were illuminated using 491-, 561-, and 640-nm lasers. All images of fixed tissue were taken at room temperature using PBS as the imaging medium.

Live imaging of mitochondrial axonal transport

Time-lapse images of mitochondrial axonal transport were captured with a spinning disk confocal unit on an inverted microscope with Perfect Focus system, motorized stage, incubation chamber for live cell imaging, electron multiplying charge coupled device camera, and MicroManager v1.4 acquisition software. Objective lenses were 10× (Plan Apochromat, NA 0.45), 20× (Plan Apochromat, NA 0.75, 423 nm/pixel), and 40× (Plan Apochromat, NA 0.95, 214 nm/pixel; Nikon). EGFP and RFP were illuminated using 491- and 561-nm lasers, respectively. Time-lapse imaging for Fig. 7 D was obtained on a widefield epifluorescence system (described in the Live imaging of $[Ca^{2+}]_i$ section) and on a high-speed widefield epifluorescence system consisting of a Ti inverted microscope (Nikon), Spectra-X Light Engine with ESio AOTF Controller (Lumencor, Inc.), Zyla sCMOS camera (Andor Technology), Perfect Focus system, motorized stage, and StageTop incubator (Okolab). Epifluorescence microscope images were recorded with NIS-Elements 4.2 acquisition software. Objective lenses with the epifluorescence microscopes were 10× (Plan Fluor, NA 0.30), 20× (Plan Apochromat, NA 0.75, 322 nm/pixel), and 40× (Plan Fluor, NA 0.75, 164 nm/pixel; Nikon). Excitation wavelengths were 485 nm to illuminate EGFP and 560 or 572 nm to illuminate RFP. Incubator settings for all axonal transport recordings were 37°C and 5% CO_2. pH stability of culture medium was verified at the beginning and end of imaging sessions.

At the beginning of each imaging session, we viewed the cultures under 10× magnification and recorded the positions of neurons with easily identifiable axons, using EGFP (FUGW) as a morphology marker. Axons were distinguished as the longest neurite (≥3 times longer than other neurites) in each neuron. The reliability of this method for identifying axons was verified in separate hippocampal neuronal cultures in which FUGW was cotransfected with BFP-synaptophysin, an axonal marker (provided by K. Nakamura, Gladstone Institute of Neurological Disease, San Francisco, CA; Berthet et al., 2014). Live imaging of axonal mitochondria (mito-RFP) was performed for each axon with a 20× or 40× objective. The 40× objective was used for most sessions. Axons were recorded for 30 min to 1 h under baseline conditions—for 30 min during any intermediate treatments (e.g., TTX [Tocris Bioscience] or SB 415286 [Tocris Bioscience]) and for 1 h during Aβ or vehicle treatments. The programmable motorized stage enabled imaging of the same axons before and during treatments. Therefore, each axon had its own corresponding baseline recording. Images of mito-RFP were obtained every 1 s for 150 s, with an exposure time of 110 ms per frame. On average, 25 mitochondria in an axon segment length of 132 µm, beginning at least 50 µm distal to the cell body, were recorded per axon.

Live imaging of $[Ca^{2+}]_i$

Calcium imaging was performed on a widefield epifluorescence system, with a Ti-E inverted microscope, broad-spectrum plasma light source (Lambda XL lamp; Sutter Instrument), motorized stage (Nikon), excitation filter wheel, and Coolsnap HQ2 CCD camera (Photometrics). Cultures were imaged inside a 37°C incubation chamber. Fura-2 imaging was acquired using a 10× objective (Plan Fluor, NA 0.3, 654 nm/pixel), 340- and 380-nm excitation filters, and a FURA2 Emission Filter (Chroma Technology Corp.). Excitation exposure times ranged from 100 to 300 ms to optimize signal brightness following published guidelines (Barreto-Chang and Dolmetsch, 2009). Images were recorded with NIS-Elements 4.2 acquisition software.

45 min before imaging, primary hippocampal neurons were placed in warm Hepes-buffered saline solution (HBS: 119 mM NaCl, 2.5mM KCl, 2 mM $MgCl_2$, 2 mM $CaCl_2$, 25 mM Hepes, and 30 mM glucose) and labeled with acetoxy-methyl-ester Fura-2 (Fura-2 AM; Invitrogen) ratiometric calcium indicator. The Fura-2 AM stock was prepared by dissolving a 50-µg vial in Pluronic F-127 (10% solution in DMSO; Invitrogen) to a concentration of 4 mM. The Fura-2 AM stock was then diluted to a final concentration of 1:1,000 in HBS for cell labeling. Immediately before imaging, the cultures were washed twice with warm HBS and then placed again in warm HBS as an imaging medium. Cells were imaged for 2–5 min under baseline conditions and then for up to 40 min after treatments. 50 mM KCl was administered at the end of each experiment as a positive control to increase $[Ca^{2+}]_i$. Images were obtained every 5 s for KCl treatments and every 30 s for Aβ treatments.

Image analysis

Axonal transport images were processed in ImageJ (National Institutes of Health) using the Multiple Kymograph and tsp050706 plugins. Investigators were blinded to genotypes and treatments. To ensure that viable cells were imaged, we excluded cells with axonal beading in EGFP and axons with no moving mitochondria during baseline conditions. Moving mitochondria were defined as those showing displacement of at least 2 µm, which is the approximate length of a mitochondrion under the conditions used here. Directionality was defined as the direction of maximum displacement. Velocity was measured for each moving mitochondrion by averaging its total velocity, including any brief pauses, while in the image frame. For bidirectionally moving mitochondria, we selected the mean velocity along the direction of maximum displacement. Lengths of mitochondria were measured on the kymographs. Pixels were converted to micrometers based on the calibration of the objective.

Calcium imaging and immunocytochemistry were quantified using NIS-Elements 4.2. Regions of interest were drawn around cell bodies to quantify Fura-2 fluorescence intensities (340/380 ratio) and around cell bodies and axons to quantify fluorescence intensity of immunocytochemically labeled neurons. Fluorescence intensity was normalized to the background signal.

Western blot analysis

Protein concentrations of lysates from primary neuronal cultures collected on DIV 14 were determined by Bradford protein assay using the Bradford reagent (Bio-Rad Laboratories) and a BSA (Thermo Fisher Scientific) standard curve. Sample absorbance and protein concentrations were read with a spectrophotometer (DU 640B; Beckman Coulter).

Western blot samples were prepared by combining NuPAGE LDS sample buffer (Invitrogen), NuPAGE sample reducing agent (Invitrogen), the protein sample, and EMD Millipore water to equate sample volumes. Wells were generally loaded with 8–15 µg of protein, except HEK293T cell lysates, which were loaded at 40 µg per well. The samples were placed on a 70°C heating block for 10 min to denature proteins and then loaded into NuPAGE Novex 4–12% Bis-Tris Midi Protein Gels (Novex) with one of the following three protein ladders on outer wells: Precision Plus Dual Color (Bio-Rad Laboratories), Precision Plus Kaleidoscope (Bio-Rad Laboratories), or BenchMark (Invitrogen). The running buffer consisted of MOPS running buffer (Invitrogen) in cold EMD Millipore water, and the gel was run at 180 V for 1 h and 10 min. Before transfer, the gel was incubated for 20 min in 2× transfer buffer consisting of NuPage transfer buffer (Novex) in EMD Millipore water with 10% methanol (Thermo Fisher Scientific). The protein transfer was completed in 9 min using an iBlot (Invitrogen) and iBlot transfer stacks (Novex). The nitrocellulose membrane was washed with TBS three times for 8 min followed by incubation in Odyssey blocking buffer (LI-COR Biosciences) for 1 h at room temperature. Membranes were incubated with primary antibodies (Table S1) diluted in 5% BSA (Sigma-Aldrich) in TBS with 0.2% Tween 20 (Bio-Rad Laboratories) overnight at 4°C. Between the primary and secondary antibody incubations, membranes were washed three times for 8 min with 0.05% Tween 20 in TBS. The membranes were then incubated for 1 h at room temperature in fluorescent secondary antibodies (Table S2), diluted in 5% BSA with 0.2% Tween 20, and washed three times for 8 min with TBS. Western blots were analyzed with an Odyssey CLx detection system and Image Studio version 2.0 (LI-COR Biosciences). To account for loading variability, all protein bands were normalized to either actin or GAPDH (Table S1).

To measure full-length hAPP and hAPP C-terminal fragments, we made the following modifications to the protocol. Protein lysates (45–50 µg) were loaded on a 10–20% Tris-Tricine gel (Bio-Rad Laboratories) with XT MES (Bio-Rad Laboratories). The gel was run at 120 V on ice until the loading dye reached the bottom of the gel. Proteins were transferred to a nitrocellulose membrane using a Criterion blotter (Sigma-Aldrich) overnight at 4°C at 0.1 A. The nitrocellulose membranes were temporarily stained with Ponceau S solution (Sigma-Aldrich) and cut at 25 kD. The top part of the membrane was blocked in 5% BSA in TBS and the bottom part of the membrane was blocked with 5% milk in TBS for 5 h at room temperature. The remainder of the protocol was performed as in the previous paragraph using 8E5 (hAPP) and anti-actin in 5% BSA in TBS plus 0.1% Tween 20 and CT15 (C-terminal fragments; provided by E.H. Koo, University of California San Diego, San Diego, CA) in 5% milk in TBS plus 0.1% Tween 20, as primary antibodies (Table S1). CT15 is a polyclonal antibody generated against a synthetic peptide corresponding to the final 15 residues of the C terminus of APP (Sisodia et al., 1993). Secondary antibodies (Table S2) were in Odyssey blocking buffer plus 0.2% Tween 20.

To characterize $A\beta_{1–42}$ oligomer preparations by Western blotting, 1 µl of NuPAGE LDS sample buffer was added to 10–100 ng of protein per well. Samples were loaded immediately onto a 10–20% Tris-Tricine gel without adding reducing agent or heating. After running the gel at 120 V for 4 h, it was transferred to a nitrocellulose membrane using an iBlot for 9 min. The membrane was microwaved in 100 ml PBS for 2.5 min and then allowed to cool for 2.5 min on the bench top. The blot was blocked in 5% BSA in TBS overnight at 4°C. The blot was incubated at room temperature in primary antibodies (82E1 and 6E10 [Table S1]) in 5% BSA in TBS plus 0.1% Tween 20

for 3 h, and then in secondary antibody (IRDye 800CW donkey anti–mouse IgG, 1:10,000) in Odyssey blocking buffer plus 0.2% Tween 20 for 1 h.

RT-qPCR

For RT-qPCR, total RNA was isolated from neuronal cultures, reverse transcribed, and analyzed by real-time PCR using the TaqMan Gene Expression Cells-to-C_T kit (Ambion) and a Sequence Detection System (ABI Prism 7900HT; Applied Biosystems). The TaqMan Assay primer–probe sets for mouse GSK3β (Mm00444911_m1) and mouse GAPDH (Mm99999915_g1) were obtained from Life Technologies. GSK3β mRNA levels were normalized to GAPDH.

Atomic force microscopy

We used ex situ atomic force microscopy as described previously (Cheng et al., 2009) to analyze the $A\beta_{1–42}$ preparations that were added to neuronal cultures. After incubation at 4°C overnight, $A\beta_{1–42}$ preparations were deposited on freshly cleaved mica (SPI Supplies) and allowed to sit for 2 min. The mica substrate was then washed with 200 µl of ultrapure water, and the sample was dried under a gentle stream of air. Samples were imaged with a scanning probe microscope (MFP3D; Asylum Research) using a silicon cantilever (Veeco) with a nominal spring constant of 40 N/m and resonance frequency of 240–270 kHz. Images were acquired using the following settings: drive amplitude 150–500 kHz with set points of 0.55–0.7 V, scan frequencies of 2–4 Hz, image resolution of 512 × 256 points, and scan size of 6.5 µm.

Statistical analysis

Individual neurons were designated as independent biological units for statistical comparisons as described previously (Vossel et al., 2010). Intergroup differences in genotype or treatment effects were assessed by one-way or two-way analysis of variance (ANOVA) followed by Dunnett's post-hoc tests (parametric data) or Kruskal-Wallis ANOVA, followed by Dunn's post-hoc tests (nonparametric data). Within each genotype group, treatment effects were assessed with paired *t* tests (parametric data) or Mann-Whitney rank-sum test (nonparametric data) with Bonferroni correction for multiple comparisons. For sequential treatments, treatment effects were compared using repeated measures ANOVA followed by Dunnett's post-hoc tests. The Levene median test for equality of variances was used to assess variance in $[Ca^{2+}]_i$. The null hypothesis was rejected at $P < 0.05$. Unadjusted p-values that survived corrections for multiple comparisons are shown in the figures. Statistical analyses were performed with SigmaPlot version 12.0 (Systat Software).

Online supplemental material

Fig. S1 shows that the velocity and length of mitochondria are unaffected by hAPP/Aβ overexpression and tau ablation. Fig. S2 characterizes the GSM and $A\beta_{1–42}$ preparations. Fig. S3 shows expression of tau truncation mutants in transfected HEK293T cells by Western blotting and in transfected *Tau*$^{-/-}$ neurons by immunocytochemistry. Fig. S4 shows that expressing the tau truncation mutants and the Y18F and AxxA7 tau mutants in *Tau*$^{-/-}$ hippocampal neurons does not affect axonal mitochondrial transport under baseline conditions. Fig. S5 shows that exposure of wild-type and *Tau*$^{-/-}$ neurons to Aβ oligomers does not change the acetylation or polyglutamylation of tubulin. Tables S1 and S2 list the details of the primary and secondary antibodies, respectively, used in this investigation. Online supplemental material is available at http://www.jcb.org/cgi/content/full/jcb.201407065/DC1.

We thank W. Guo, J. Kang, S. Lee, T. Sweeney, and X. Wang for excellent technical support; L. Mitic, K. Thorn, D. Larsen, the Consortium for Frontotemporal Dementia Research, and the Nikon Imaging Center for microscopy support; E. LaDow and L. Zhu for advice on calcium imaging; S. Maeda for advice on plasmid construction and tau antibodies; J. Harris for lentiviral vectors; H. Dawson and M. Vitek for *Tau* knockout mice; D. Zuev, L. Thompson, and J. Toyn for the GSM; L. Gan for the FUGW plasmid; Y. Yoon for the mito-RFP plasmid; K. Nakamura for the BFP-synaptophysin plasmid; E. Koo for the CT15 antibody; and A. Cheung and M. Dela Cruz for administrative assistance.

The study was supported by National Institutes of Health grants K23 AG038357 (to K.A. Vossel) and NS041787 (to L. Mucke); the John Douglas French Alzheimer's Foundation (to K.A. Vossel); and a gift from the S. D. Bechtel, Jr. Foundation. L. Mucke has received research funding for other projects from Bristol-Myers Squibb.

The authors declare no further competing financial interests.

Submitted: 15 July 2014
Accepted: 2 April 2015

References

Agarwal-Mawal, A., H.Y. Qureshi, P.W. Cafferty, Z. Yuan, D. Han, R. Lin, and H.K. Paudel. 2003. 14-3-3 connects glycogen synthase kinase-3β to tau within a brain microtubule-associated tau phosphorylation complex. *J. Biol. Chem.* 278:12722–12728. http://dx.doi.org/10.1074/jbc.M211491200

Albright, C.F., R.C. Dockens, J.E. Meredith Jr., R.E. Olson, R. Slemmon, K.A. Lentz, J.S. Wang, R.R. Denton, G. Pilcher, P.W. Rhyne, et al. 2013. Pharmacodynamics of selective inhibition of γ-secretase by avagacestat. *J. Pharmacol. Exp. Ther.* 344:686–695. http://dx.doi.org/10.1124/jpet.112.199356

Augustinack, J.C., A. Schneider, E.M. Mandelkow, and B.T. Hyman. 2002. Specific tau phosphorylation sites correlate with severity of neuronal cytopathology in Alzheimer's disease. *Acta Neuropathol.* 103:26–35. http://dx.doi.org/10.1007/s004010100423

Barbosa, D.J., R. Serrat, S. Mirra, M. Quevedo, E. Gómez de Barreda, J. Avila, E. Fernandes, M.L. Bastos, J.P. Capela, F. Carvalho, and E. Soriano. 2014. MDMA impairs mitochondrial neuronal trafficking in a Tau- and Mitofusin2/Drp1-dependent manner. *Arch. Toxicol.* 88:1561–1572. http://dx.doi.org/10.1007/s00204-014-1209-7

Barnes, S.J., T. Opitz, M. Merkens, T. Kelly, C. von der Brelie, R. Krueppel, and H. Beck. 2010. Stable mossy fiber long-term potentiation requires calcium influx at the granule cell soma, protein synthesis, and microtubule-dependent axonal transport. *J. Neurosci.* 30:12996–13004. http://dx.doi.org/10.1523/JNEUROSCI.1847-10.2010

Barreto-Chang, O.L., and R.E. Dolmetsch. 2009. Calcium imaging of cortical neurons using Fura-2 AM. *J. Vis. Exp.* 19:1067. http://dx.doi.org/10.3791/1067

Berthet, A., E.B. Margolis, J. Zhang, I. Hsieh, J. Zhang, T.S. Hnasko, J. Ahmad, R.H. Edwards, H. Sesaki, E.J. Huang, and K. Nakamura. 2014. Loss of mitochondrial fission depletes axonal mitochondria in midbrain dopamine neurons. *J. Neurosci.* 34:14304–14317. http://dx.doi.org/10.1523/JNEUROSCI.0930-14.2014

Boy, K.M., J.M. Guernon, J.E. Macor, R.E. Olson, J. Shi, L.A. Thompson III, Y. Wu, L. Xu, Y. Zhang, and D.S. Zuev. 2013. Compounds for the reduction of β-amyloid production. United States patent US 8486952 B2, Example 7A, filed July 28, 2010 and issued July 16, 2013.

Brady, S.T., M. Tytell, and R.J. Lasek. 1984. Axonal tubulin and axonal microtubules: biochemical evidence for cold stability. *J. Cell Biol.* 99:1716–1724. http://dx.doi.org/10.1083/jcb.99.5.1716

Busche, M.A., G. Eichhoff, H. Adelsberger, D. Abramowski, K.H. Wiederhold, C. Haass, M. Staufenbiel, A. Konnerth, and O. Garaschuk. 2008. Clusters of hyperactive neurons near amyloid plaques in a mouse model of Alzheimer's disease. *Science*. 321:1686–1689. http://dx.doi.org/10.1126/science.1162844

Calkins, M.J., and P.H. Reddy. 2011. Amyloid beta impairs mitochondrial anterograde transport and degenerates synapses in Alzheimer's disease neurons. *Biochim. Biophys. Acta*. 1812:507–513. http://dx.doi.org/10.1016/j.bbadis.2011.01.007

Caricasole, A., A. Copani, F. Caraci, E. Aronica, A.J. Rozemuller, A. Caruso, M. Storto, G. Gaviraghi, G.C. Terstappen, and F. Nicoletti. 2004. Induction of Dickkopf-1, a negative modulator of the Wnt pathway, is associated with neuronal degeneration in Alzheimer's brain. *J. Neurosci.* 24:6021–6027. http://dx.doi.org/10.1523/JNEUROSCI.1381-04.2004

Cheng, J.S., D.B. Dubal, D.H. Kim, J. Legleiter, I.H. Cheng, G.Q. Yu, I. Tesseur, T. Wyss-Coray, P. Bonaldo, and L. Mucke. 2009. Collagen VI protects neurons against Aβ toxicity. *Nat. Neurosci.* 12:119–121. http://dx.doi.org/10.1038/nn.2240

Cho, D.H., T. Nakamura, J. Fang, P. Cieplak, A. Godzik, Z. Gu, and S.A. Lipton. 2009. S-nitrosylation of Drp1 mediates β-amyloid–related mitochondrial fission and neuronal injury. *Science*. 324:102–105. http://dx.doi.org/10.1126/science.1171091

Cissé, M., B. Halabisky, J. Harris, N. Devidze, D.B. Dubal, B. Sun, A. Orr, G. Lotz, D.H. Kim, P. Hamto, et al. 2011. Reversing EphB2 depletion rescues cognitive functions in Alzheimer model. *Nature*. 469:47–52. http://dx.doi.org/10.1038/nature09635

Coghlan, M.P., A.A. Culbert, D.A. Cross, S.L. Corcoran, J.W. Yates, N.J. Pearce, O.L. Rausch, G.J. Murphy, P.S. Carter, L. Roxbee Cox, et al. 2000. Selective small molecule inhibitors of glycogen synthase kinase-3 modulate glycogen metabolism and gene transcription. *Chem. Biol.* 7:793–803. http://dx.doi.org/10.1016/S1074-5521(00)00025-9

Cross, D.A., A.A. Culbert, K.A. Chalmers, L. Facci, S.D. Skaper, and A.D. Reith. 2001. Selective small-molecule inhibitors of glycogen synthase kinase-3 activity protect primary neurones from death. *J. Neurochem.* 77:94–102. http://dx.doi.org/10.1046/j.1471-4159.2001.t01-1-00251.x

Dawson, H.N., A. Ferreira, M.V. Eyster, N. Ghoshal, L.I. Binder, and M.P. Vitek. 2001. Inhibition of neuronal maturation in primary hippocampal neurons from tau deficient mice. *J. Cell Sci.* 114:1179–1187.

Decker, H., K.Y. Lo, S.M. Unger, S.T. Ferreira, and M.A. Silverman. 2010. Amyloid-β peptide oligomers disrupt axonal transport through an NMDA receptor-dependent mechanism that is mediated by glycogen synthase kinase 3β in primary cultured hippocampal neurons. *J. Neurosci.* 30:9166–9171. http://dx.doi.org/10.1523/JNEUROSCI.1074-10.2010

De Felice, F.G., P.T. Velasco, M.P. Lambert, K. Viola, S.J. Fernandez, S.T. Ferreira, and W.L. Klein. 2007. Aβ oligomers induce neuronal oxidative stress through an *N*-methyl-D-aspartate receptor-dependent mechanism that is blocked by the Alzheimer drug memantine. *J. Biol. Chem.* 282:11590–11601. http://dx.doi.org/10.1074/jbc.M607483200

DeVos, S.L., D.K. Goncharoff, G. Chen, C.S. Kebodeaux, K. Yamada, F.R. Stewart, D.R. Schuler, S.E. Maloney, D.F. Wozniak, F. Rigo, et al. 2013. Antisense reduction of tau in adult mice protects against seizures. *J. Neurosci.* 33:12887–12897. http://dx.doi.org/10.1523/JNEUROSCI.2107-13.2013

DuBoff, B., J. Götz, and M.B. Feany. 2012. Tau promotes neurodegeneration via DRP1 mislocalization in vivo. *Neuron*. 75:618–632. http://dx.doi.org/10.1016/j.neuron.2012.06.026

Gheyara, A.L., R. Ponnusamy, B. Djukic, R.J. Craft, K. Ho, W. Guo, M.M. Finucane, P.E. Sanchez, and L. Mucke. 2014. Tau reduction prevents disease in a mouse model of Dravet syndrome. *Ann. Neurol.* 76:443–456. http://dx.doi.org/10.1002/ana.24230

He, H.J., X.S. Wang, R. Pan, D.L. Wang, M.N. Liu, and R.Q. He. 2009. The proline-rich domain of tau plays a role in interactions with actin. *BMC Cell Biol.* 10:81. http://dx.doi.org/10.1186/1471-2121-10-81

Hiruma, H., T. Katakura, S. Takahashi, T. Ichikawa, and T. Kawakami. 2003. Glutamate and amyloid β-protein rapidly inhibit fast axonal transport in cultured rat hippocampal neurons by different mechanisms. *J. Neurosci.* 23:8967–8977.

Holth, J.K., V.C. Bomben, J.G. Reed, T. Inoue, L. Younkin, S.G. Younkin, R.G. Pautler, J. Botas, and J.L. Noebels. 2013. Tau loss attenuates neuronal network hyperexcitability in mouse and *Drosophila* genetic models of epilepsy. *J. Neurosci.* 33:1651–1659. http://dx.doi.org/10.1523/JNEUROSCI.3191-12.2013

Ittner, L.M., T. Fath, Y.D. Ke, M. Bi, J. van Eersel, K.M. Li, P. Gunning, and J. Götz. 2008. Parkinsonism and impaired axonal transport in a mouse model of frontotemporal dementia. *Proc. Natl. Acad. Sci. USA*. 105:15997–16002. http://dx.doi.org/10.1073/pnas.0808084105

Ittner, L.M., Y.D. Ke, F. Delerue, M. Bi, A. Gladbach, J. van Eersel, H. Wölfing, B.C. Chieng, M.J. Christie, I.A. Napier, et al. 2010. Dendritic function of tau mediates amyloid-β toxicity in Alzheimer's disease mouse models. *Cell*. 142:387–397. http://dx.doi.org/10.1016/j.cell.2010.06.036

Jin, M., N. Shepardson, T. Yang, G. Chen, D. Walsh, and D.J. Selkoe. 2011. Soluble amyloid β-protein dimers isolated from Alzheimer cortex directly induce Tau hyperphosphorylation and neuritic degeneration. *Proc. Natl. Acad. Sci. USA*. 108:5819–5824. http://dx.doi.org/10.1073/pnas.1017033108

Jo, J., D.J. Whitcomb, K.M. Olsen, T.L. Kerrigan, S.C. Lo, G. Bru-Mercier, B. Dickinson, S. Scullion, M. Sheng, G. Collingridge, and K. Cho. 2011. $A\beta_{1-42}$ inhibition of LTP is mediated by a signaling pathway involving caspase-3, Akt1 and GSK-3β. *Nat. Neurosci.* 14:545–547. http://dx.doi.org/10.1038/nn.2785

Johnson-Wood, K., M. Lee, R. Motter, K. Hu, G. Gordon, R. Barbour, K. Khan, M. Gordon, H. Tan, D. Games, et al. 1997. Amyloid precursor protein processing and $A\beta_{42}$ deposition in a transgenic mouse model of Alzheimer disease. *Proc. Natl. Acad. Sci. USA*. 94:1550–1555. http://dx.doi.org/10.1073/pnas.94.4.1550

Kanaan, N.M., G.A. Morfini, N.E. LaPointe, G.F. Pigino, K.R. Patterson, Y. Song, A. Andreadis, Y. Fu, S.T. Brady, and L.I. Binder. 2011. Pathogenic forms of tau inhibit kinesin-dependent axonal transport through a mechanism involving activation of axonal phosphotransferases. *J. Neurosci.* 31:9858–9868. http://dx.doi.org/10.1523/JNEUROSCI.0560-11.2011

Kanaan, N.M., G. Morfini, G. Pigino, N.E. LaPointe, A. Andreadis, Y. Song, E. Leitman, L.I. Binder, and S.T. Brady. 2012. Phosphorylation in the amino terminus of tau prevents inhibition of anterograde axonal transport. *Neurobiol. Aging*. 33:e15–e30. http://dx.doi.org/10.1016/j.neurobiolaging.2011.06.006

Kelly, B.L., and A. Ferreira. 2006. β-Amyloid-induced dynamin 1 degradation is mediated by *N*-methyl-D-aspartate receptors in hippocampal neurons. *J. Biol. Chem.* 281:28079–28089. http://dx.doi.org/10.1074/jbc.M605081200

Kessels, H.W., S. Nabavi, and R. Malinow. 2013. Metabotropic NMDA receptor function is required for β-amyloid–induced synaptic depression. *Proc. Natl. Acad. Sci. USA*. 110:4033–4038. http://dx.doi.org/10.1073/pnas.1219605110

Kimura, T., D.J. Whitcomb, J. Jo, P. Regan, T. Piers, S. Heo, C. Brown, T. Hashikawa, M. Murayama, H. Seok, et al. 2014. Microtubule-associated protein tau is essential for long-term depression in the hippocampus. *Philos. Trans. R. Soc. Lond. B Biol. Sci.* 369:20130144. http://dx.doi.org/10.1098/rstb.2013.0144

King, M.E., H.M. Kan, P.W. Baas, A. Erisir, C.G. Glabe, and G.S. Bloom. 2006. Tau-dependent microtubule disassembly initiated by prefibrillar β-amyloid. *J. Cell Biol.* 175:541–546. http://dx.doi.org/10.1083/jcb.200605187

Kondadi, A.K., S. Wang, S. Montagner, N. Kladt, A. Korwitz, P. Martinelli, D. Herholz, M.J. Baker, A.C. Schauss, T. Langer, and E.I. Rugarli. 2014. Loss of the m-AAA protease subunit AFG_3L_2 causes mitochondrial transport defects and tau hyperphosphorylation. *EMBO J.* 33:1011–1026. http://dx.doi.org/10.1002/embj.201387009

LaPointe, N.E., G. Morfini, G. Pigino, I.N. Gaisina, A.P. Kozikowski, L.I. Binder, and S.T. Brady. 2009. The amino terminus of tau inhibits kinesin-dependent axonal transport: implications for filament toxicity. *J. Neurosci. Res.* 87:440–451. http://dx.doi.org/10.1002/jnr.21850

Lardong, K., C. Maas, and M. Kneussel. 2009. Neuronal depolarization modifies motor protein mobility. *Neuroscience*. 160:1–5. http://dx.doi.org/10.1016/j.neuroscience.2009.02.034

Lee, G., S.T. Newman, D.L. Gard, H. Band, and G. Panchamoorthy. 1998. Tau interacts with src-family non-receptor tyrosine kinases. *J. Cell Sci.* 111:3167–3177.

Lee, G., R. Thangavel, V.M. Sharma, J.M. Litersky, K. Bhaskar, S.M. Fang, L.H. Do, A. Andreadis, G. Van Hoesen, and H. Ksiezak-Reding. 2004. Phosphorylation of tau by fyn: implications for Alzheimer's disease. *J. Neurosci.* 24:2304–2312. http://dx.doi.org/10.1523/JNEUROSCI.4162-03.2004

Leroy, K., K. Ando, V. Laporte, R. Dedecker, V. Suain, M. Authelet, C. Héraud, N. Pierrot, Z. Yilmaz, J.N. Octave, and J.P. Brion. 2012. Lack of tau proteins rescues neuronal cell death and decreases amyloidogenic processing of APP in APP/PS1 mice. *Am. J. Pathol.* 181:1928–1940. http://dx.doi.org/10.1016/j.ajpath.2012.08.012

Leugers, C.J., and G. Lee. 2010. Tau potentiates nerve growth factor-induced mitogen-activated protein kinase signaling and neurite initiation without a requirement for microtubule binding. *J. Biol. Chem.* 285:19125–19134. http://dx.doi.org/10.1074/jbc.M110.105387

Li, S., S. Hong, N.E. Shepardson, D.M. Walsh, G.M. Shankar, and D. Selkoe. 2009. Soluble oligomers of amyloid β protein facilitate hippocampal long-term depression by disrupting neuronal glutamate uptake. *Neuron*. 62:788–801. http://dx.doi.org/10.1016/j.neuron.2009.05.012

Lois, C., E.J. Hong, S. Pease, E.J. Brown, and D. Baltimore. 2002. Germline transmission and tissue-specific expression of transgenes delivered by lentiviral vectors. *Science*. 295:868–872. http://dx.doi.org/10.1126/science.1067081

McMillan, P., E. Korvatska, P. Poorkaj, Z. Evstafjeva, L. Robinson, L. Greenup, J. Leverenz, G.D. Schellenberg, and I. D'Souza. 2008. Tau isoform regulation is region- and cell-specific in mouse brain. *J. Comp. Neurol.* 511:788–803. http://dx.doi.org/10.1002/cne.21867

Miao, Y., J. Chen, Q. Zhang, and A. Sun. 2010. Deletion of *tau* attenuates heat shock-induced injury in cultured cortical neurons. *J. Neurosci. Res.* 88:102–110. http://dx.doi.org/10.1002/jnr.22188

Morfini, G., G. Szebenyi, R. Elluru, N. Ratner, and S.T. Brady. 2002. Glycogen synthase kinase 3 phosphorylates kinesin light chains and negatively regulates kinesin-based motility. *EMBO J.* 21:281–293. http://dx.doi.org/10.1093/emboj/21.3.281

Morris, M., S. Maeda, K. Vossel, and L. Mucke. 2011. The many faces of tau. *Neuron*. 70:410–426. http://dx.doi.org/10.1016/j.neuron.2011.04.009

Morris, M., P. Hamto, A. Adame, N. Devidze, E. Masliah, and L. Mucke. 2013. Age-appropriate cognition and subtle dopamine-independent motor deficits in aged tau knockout mice. *Neurobiol. Aging*. 34:1523–1529. http://dx.doi.org/10.1016/j.neurobiolaging.2012.12.003

Mucke, L., E. Masliah, G.-Q. Yu, M. Mallory, E.M. Rockenstein, G. Tatsuno, K. Hu, D. Kholodenko, K. Johnson-Wood, and L. McConlogue. 2000. High-level neuronal expression of $A\beta_{1-42}$ in wild-type human amyloid protein precursor transgenic mice: synaptotoxicity without plaque formation. *J. Neurosci.* 20:4050–4058.

Nakayama, T., and T. Sawada. 2002. Involvement of microtubule integrity in memory impairment caused by colchicine. *Pharmacol. Biochem. Behav.* 71:119–138. http://dx.doi.org/10.1016/S0091-3057(01)00634-7

Nguyen, T.T., S.S. Oh, D. Weaver, A. Lewandowska, D. Maxfield, M.H. Schuler, N.K. Smith, J. Macfarlane, G. Saunders, C.A. Palmer, et al. 2014. Loss of Miro1-directed mitochondrial movement results in a novel murine model for neuron disease. *Proc. Natl. Acad. Sci. USA*. 111:E3631–E3640. http://dx.doi.org/10.1073/pnas.1402449111

Nussbaum, J.M., S. Schilling, H. Cynis, A. Silva, E. Swanson, T. Wangsanut, K. Tayler, B. Wiltgen, A. Hatami, R. Rönicke, et al. 2012. Prion-like behaviour and tau-dependent cytotoxicity of pyroglutamylated amyloid-β. *Nature*. 485:651–655. http://dx.doi.org/10.1038/nature11060

Peineau, S., C. Taghibiglou, C. Bradley, T.P. Wong, L. Liu, J. Lu, E. Lo, D. Wu, E. Saule, T. Bouschet, et al. 2007. LTP inhibits LTD in the hippocampus via regulation of GSK3β. *Neuron*. 53:703–717. http://dx.doi.org/10.1016/j.neuron.2007.01.029

Peruzzi, P.P., S.E. Lawler, S.L. Senior, N. Dmitrieva, P.A. Edser, D. Gianni, E.A. Chiocca, and R. Wade-Martins. 2009. Physiological transgene regulation and functional complementation of a neurological disease gene deficiency in neurons. *Mol. Ther.* 17:1517–1526. http://dx.doi.org/10.1038/mt.2009.64

Preuss, U., J. Biernat, E.M. Mandelkow, and E. Mandelkow. 1997. The 'jaws' model of tau-microtubule interaction examined in CHO cells. *J. Cell Sci.* 110:789–800.

Ramser, E.M., K.J. Gan, H. Decker, E.Y. Fan, M.M. Suzuki, S.T. Ferreira, and M.A. Silverman. 2013. Amyloid-β oligomers induce tau-independent disruption of BDNF axonal transport via calcineurin activation in cultured hippocampal neurons. *Mol. Biol. Cell*. 24:2494–2505. http://dx.doi.org/10.1091/mbc.E12-12-0858

Rapoport, M., H.N. Dawson, L.I. Binder, M.P. Vitek, and A. Ferreira. 2002. Tau is essential to β-amyloid-induced neurotoxicity. *Proc. Natl. Acad. Sci. USA*. 99:6364–6369. http://dx.doi.org/10.1073/pnas.092136199

Renner, M., P.N. Lacor, P.T. Velasco, J. Xu, A. Contractor, W.L. Klein, and A. Triller. 2010. Deleterious effects of amyloid β oligomers acting as an extracellular scaffold for mGluR5. *Neuron*. 66:739–754. http://dx.doi.org/10.1016/j.neuron.2010.04.029

Reynolds, C.H., C.J. Garwood, S. Wray, C. Price, S. Kellie, T. Perera, M. Zvelebil, A. Yang, P.W. Sheppard, I.M. Varndell, et al. 2008. Phosphorylation regulates tau interactions with Src homology 3 domains of phosphatidylinositol 3-kinase, phospholipase Cγ1, Grb2, and Src family kinases. *J. Biol. Chem.* 283:18177–18186. http://dx.doi.org/10.1074/jbc.M709715200

Roberson, E.D., K. Scearce-Levie, J.J. Palop, F. Yan, I.H. Cheng, T. Wu, H. Gerstein, G.-Q. Yu, and L. Mucke. 2007. Reducing endogenous tau ameliorates amyloid β-induced deficits in an Alzheimer's disease mouse model. *Science*. 316:750–754. http://dx.doi.org/10.1126/science.1141736

Roberson, E.D., B. Halabisky, J.W. Yoo, J. Yao, J. Chin, F. Yan, T. Wu, P. Hamto, N. Devidze, G.-Q. Yu, et al. 2011. Amyloid-β/Fyn–induced synaptic, network, and cognitive impairments depend on tau levels in multiple mouse models of Alzheimer's disease. *J. Neurosci.* 31:700–711. http://dx.doi.org/10.1523/JNEUROSCI.4152-10.2011

Rui, Y., P. Tiwari, Z. Xie, and J.Q. Zheng. 2006. Acute impairment of mitochondrial trafficking by β-amyloid peptides in hippocampal neurons. *J. Neurosci.* 26:10480–10487. http://dx.doi.org/10.1523/JNEUROSCI.3231-06.2006

Sanchez-Mejia, R.O., J.W. Newman, S. Toh, G.-Q. Yu, Y. Zhou, B. Halabisky, M. Cissé, K. Scearce-Levie, I.H. Cheng, L. Gan, et al. 2008. Phospholipase A2 reduction ameliorates cognitive deficits in a mouse model of Alzheimer's disease. *Nat. Neurosci.* 11:1311–1318. http://dx.doi.org/10.1038/nn.2213

Sapir, T., M. Frotscher, T. Levy, E.M. Mandelkow, and O. Reiner. 2012. Tau's role in the developing brain: implications for intellectual disability. *Hum. Mol. Genet.* 21:1681–1692. http://dx.doi.org/10.1093/hmg/ddr603

Seward, M.E., E. Swanson, A. Norambuena, A. Reimann, J.N. Cochran, R. Li, E.D. Roberson, and G.S. Bloom. 2013. Amyloid-β signals through tau to drive ectopic neuronal cell cycle re-entry in Alzheimer's disease. *J. Cell Sci.* 126:1278–1286. http://dx.doi.org/10.1242/jcs.1125880

Shahpasand, K., I. Uemura, T. Saito, T. Asano, K. Hata, K. Shibata, Y. Toyoshima, M. Hasegawa, and S. Hisanaga. 2012. Regulation of mitochondrial transport and inter-microtubule spacing by tau phosphorylation at the sites hyperphosphorylated in Alzheimer's disease. *J. Neurosci.* 32:2430–2441. http://dx.doi.org/10.1523/JNEUROSCI.5927-11.2012

Shipton, O.A., J.R. Leitz, J. Dworzak, C.E.J. Acton, E.M. Tunbridge, F. Denk, H.N. Dawson, M.P. Vitek, R. Wade-Martins, O. Paulsen, and M. Vargas-Caballero. 2011. Tau protein is required for amyloid β-induced impairment of hippocampal long-term potentiation. *J. Neurosci.* 31:1688–1692. http://dx.doi.org/10.1523/JNEUROSCI.2610-10.2011

Sisodia, S.S., E.H. Koo, P.N. Hoffman, G. Perry, and D.L. Price. 1993. Identification and transport of full-length amyloid precursor proteins in rat peripheral nervous system. *J. Neurosci.* 13:3136–3142.

Snyder, E.M., Y. Nong, C.G. Almeida, S. Paul, T. Moran, E.Y. Choi, A.C. Nairn, M.W. Salter, P.J. Lombroso, G.K. Gouras, and P. Greengard. 2005. Regulation of NMDA receptor trafficking by amyloid-β. *Nat. Neurosci.* 8:1051–1058. http://dx.doi.org/10.1038/nn1503

Söderberg, O., M. Gullberg, M. Jarvius, K. Ridderstråle, K.J. Leuchowius, J. Jarvius, K. Wester, P. Hydbring, F. Bahram, L.G. Larsson, and U. Landegren. 2006. Direct observation of individual endogenous protein complexes in situ by proximity ligation. *Nat. Methods*. 3:995–1000. http://dx.doi.org/10.1038/nmeth947

Song, Y., L.L. Kirkpatrick, A.B. Schilling, D.L. Helseth, N. Chabot, J.W. Keillor, G.V. Johnson, and S.T. Brady. 2013. Transglutaminase and polyamination of tubulin: posttranslational modification for stabilizing axonal microtubules. *Neuron*. 78:109–123. http://dx.doi.org/10.1016/j.neuron.2013.01.036

Suberbielle, E., P.E. Sanchez, A.V. Kravitz, X. Wang, K. Ho, K. Eilertson, N. Devidze, A.C. Kreitzer, and L. Mucke. 2013. Physiologic brain activity causes DNA double-strand breaks in neurons, with exacerbation by amyloid-β. *Nat. Neurosci.* 16:613–621. http://dx.doi.org/10.1038/nn.3356

Sun, W., H.Y. Qureshi, P.W. Cafferty, K. Sobue, A. Agarwal-Mawal, K.D. Neufield, and H.K. Paudel. 2002. Glycogen synthase kinase-3β is complexed with tau protein in brain microtubules. *J. Biol. Chem.* 277:11933–11940. http://dx.doi.org/10.1074/jbc.M107182200

Sutherland, C., I.A. Leighton, and P. Cohen. 1993. Inactivation of glycogen synthase kinase-3β by phosphorylation: new kinase connections in insulin and growth-factor signalling. *Biochem. J.* 296:15–19.

Takashima, A., K. Noguchi, G. Michel, M. Mercken, M. Hoshi, K. Ishiguro, and K. Imahori. 1996. Exposure of rat hippocampal neurons to amyloid β peptide (25–35) induces the inactivation of phosphatidyl inositol-3 kinase and the activation of tau protein kinase I/glycogen synthase kinase-3β. *Neurosci. Lett.* 203:33–36. http://dx.doi.org/10.1016/0304-3940(95)12257-5

Talantova, M., S. Sanz-Blasco, X. Zhang, P. Xia, M.W. Akhtar, S. Okamoto, G. Dziewczapolski, T. Nakamura, G. Cao, A.E. Pratt, et al. 2013. Aβ induces astrocytic glutamate release, extrasynaptic NMDA receptor activation, and synaptic loss. *Proc. Natl. Acad. Sci. USA*. 110:E2518–E2527. http://dx.doi.org/10.1073/pnas.1306832110

Tang, Y., D.A. Scott, U. Das, S.D. Edland, K. Radomski, E.H. Koo, and S. Roy. 2012. Early and selective impairments in axonal transport kinetics of synaptic cargoes induced by soluble amyloid β-protein oligomers. *Traffic*. 13:681–693. http://dx.doi.org/10.1111/j.1600-0854.2012.01340.x

Terwel, D., D. Muyllaert, I. Dewachter, P. Borghgraef, S. Croes, H. Devijver, and F. Van Leuven. 2008. Amyloid activates GSK-3β to aggravate neuronal tauopathy in bigenic mice. *Am. J. Pathol.* 172:786–798. http://dx.doi.org/10.2353/ajpath.2008.070904

Trepanier, C.H., M.F. Jackson, and J.F. MacDonald. 2012. Regulation of NMDA receptors by the tyrosine kinase Fyn. *FEBS J.* 279:12–19. http://dx.doi.org/10.1111/j.1742-4658.2011.08391.x

Vossel, K.A., K. Zhang, J. Brodbeck, A.C. Daub, P. Sharma, S. Finkbeiner, B. Cui, and L. Mucke. 2010. Tau reduction prevents Aβ-induced defects in axonal transport. *Science*. 330:198. http://dx.doi.org/10.1126/science.1194653

Wang, F.H., P. Appelkvist, T. Klason, O. Gissberg, A. Bogstedt, K. Eliason, S. Martinsson, S. Briem, A. Andersson, S.A. Visser, et al. 2012. Decreased axonal transport rates in the Tg2576 APP transgenic mouse: improvement with the γ-secretase inhibitor MRK-560 as detected by manganese-enhanced MRI. *Eur. J. Neurosci.* 36:3165–3172. http://dx.doi.org/10.1111/j.1460-9568.2012.08258.x

Wang, X., and T.L. Schwarz. 2009. The mechanism of Ca^{2+} -dependent regulation of kinesin-mediated mitochondrial motility. *Cell.* 136:163–174. http://dx.doi.org/10.1016/j.cell.2008.11.046

Wang, X., B. Su, S.L. Siedlak, P.I. Moreira, H. Fujioka, Y. Wang, G. Casadesus, and X. Zhu. 2008. Amyloid-β overproduction causes abnormal mitochondrial dynamics via differential modulation of mitochondrial fission/fusion proteins. *Proc. Natl. Acad. Sci. USA*. 105:19318–19323. http://dx.doi.org/10.1073/pnas.0804871105

Wang, X., B. Su, H.G. Lee, X. Li, G. Perry, M.A. Smith, and X. Zhu. 2009. Impaired balance of mitochondrial fission and fusion in Alzheimer's disease. *J. Neurosci.* 29:9090–9103. http://dx.doi.org/10.1523/JNEUROSCI.1357-09.2009

Wang, X., G. Perry, M.A. Smith, and X. Zhu. 2010. Amyloid-β-derived diffusible ligands cause impaired axonal transport of mitochondria in neurons. *Neurodegener. Dis.* 7:56–59. http://dx.doi.org/10.1159/000283484

Yoon, Y., E.W. Krueger, B.J. Oswald, and M.A. McNiven. 2003. The mitochondrial protein hFis1 regulates mitochondrial fission in mammalian cells through an interaction with the dynamin-like protein DLP1. *Mol. Cell. Biol.* 23:5409–5420. http://dx.doi.org/10.1128/MCB.23.15.5409-5420.2003

Yu, J.Z., and M.M. Rasenick. 2006. Tau associates with actin in differentiating PC12 cells. *FASEB J.* 20:1452–1461. http://dx.doi.org/10.1096/fj.05-5206com

Yuan, A., A. Kumar, C. Peterhoff, K. Duff, and R.-A. Nixon. 2008. Axonal transport rates *in vivo* are unaffected by tau deletion or overexpression in mice. *J. Neurosci.* 28:1682–1687. http://dx.doi.org/10.1523/JNEUROSCI.5242-07.2008

Zempel, H., E. Thies, E. Mandelkow, and E.M. Mandelkow. 2010. Aβ oligomers cause localized Ca^{2+} elevation, missorting of endogenous Tau into dendrites, Tau phosphorylation, and destruction of microtubules and spines. *J. Neurosci.* 30:11938–11950. http://dx.doi.org/10.1523/JNEUROSCI.2357-10.2010

Zempel, H., J. Luedtke, Y. Kumar, J. Biernat, H. Dawson, E. Mandelkow, and E.M. Mandelkow. 2013. Amyloid-β oligomers induce synaptic damage via Tau-dependent microtubule severing by TTLL6 and spastin. *EMBO J.* 32:2920–2937. http://dx.doi.org/10.1038/emboj.2013.207

Zhang, B., M. Higuchi, Y. Yoshiyama, T. Ishihara, M.S. Forman, D. Martinez, S. Joyce, J.Q. Trojanowski, and V.M. Lee. 2004. Retarded axonal transport of R406W mutant tau in transgenic mice with a neurodegenerative tauopathy. *J. Neurosci.* 24:4657–4667. http://dx.doi.org/10.1523/JNEUROSCI.0797-04.2004